CHEMISTRY
A EUROPEAN JOURNAL

DOI: 10.1002/chem.200500765

VIP

The Versatility of Pentalene Coordination to Transition Metals: A Density Functional Theory Investigation

Saïda Bendjaballah, Samia Kahlal, Karine Costuas, Emile Bévillon, and Jean-Yves Saillard*[a]

Abstract: DFT calculations with full geometry optimization have been carried out on a series of real and hypothetical compounds of the type $[CpM(C_8H_6)]$, $[(CO)_3M(C_8H_6)]$, $[M(C_8H_6)_2]$, $[(CpM)_2(C_8H_6)]$, $[\{(CO)_3M\}_2(C_8H_6)]$, and $[M_2(C_8H_6)_2]$ (M = transition metal). The bonding in all the currently known compounds is rationalized, as well as in the (so far) hypothetical stable complexes. Depending on the electron count and the nature of the metal(s), η^2 (predicted), η^3, η^5, η^8, or intermediate coordination modes can be adopted. In the case of the mononuclear species, the most favored closed-shell electron counts are 18 and 16 metal valence electrons (MVE). In the case of the dinuclear species, an electron count of 34 MVEs is most favored. However, other electron counts can be stabilized, especially in the case of dinuclear complexes. Coordinated pentalene should most often be considered as formally being a dianion, but sometimes as a neutral ligand. In the former case it can behave as an aromatic species made of two equivalent fused rings, as a C_5 aromatic ring connected to an allylic anion, or even as two allylic anions bridged by a C7=C8 double bond. In the latter case, it can behave as a bond-alternating cyclic polyene or as a C_5 aromatic ring connected to an allylic cation.

Keywords: coordination modes · density functional calculations · electron count · pentalene · transition metals

Introduction

Neutral pentalene (C_8H_6, Scheme 1) has been known for a long time to be a rather unstable molecule.[1] It can be stabilized in its aromatic 10-π-electron dianionic form (Scheme 1)[2] or by complexation to transition- or rare-earth metals.[3] In the second case, pentalene is generally considered to formally be a $C_8H_6^{2-}$ complexed dianion. Therefore, complexation is believed to provide additional stabilization to the aromatic dianion in the same way as it does for the aromatic cyclopentadienyl monoanion. Although transition-metal complexes of pentalene[4–6] have been known for a very long time since the pioneering work of Katz and coworkers,[4] recent years have seen the characterization of new compounds, most of them by the groups of Manriquez,[7] Jonas,[8] Cloke,[9] and O'Hare.[10] The structural chemistry of transition-metal pentalene compounds is particularly rich. Pentalene has been shown to bind to one, two,[3] and even three[10c] metal centers with a coordination mode that varies from η^8 to η^3. Although theoretical studies on some pentalene transition-metal complexes have been published in the past,[7a,8d,9d,e,g,11–15] no complete rationalization of the bonding in pentalene complexes with respect to their electron count and to the nature of the metals and other li-

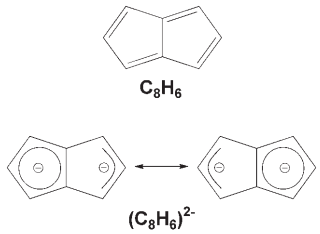

Scheme 1. Neutral pentalene (C_8H_6; top) and its stabilized aromatic 10-π-electron dianionic form $(C_8H_6)^{2-}$ (bottom).

[a] Dr. S. Bendjaballah, Dr. S. Kahlal, Dr. K. Costuas, E. Bévillon, Prof. J.-Y. Saillard
Laboratoire de Chimie du Solide et Inorganique Moléculaire
UMR CNRS 6511, Institut de Chimie de Rennes, Université de Rennes 1
35042 Rennes Cedex (France)
Fax: (+33) 223-236-840
E-mail: saillard@univ-rennes1.fr

Supporting information for this article is available on the WWW under http://www.chemeurj.org/ or from the author. A list of Cartesian coordinates and total bonding energies for the optimized geometries of the computed compounds.

gands has been provided so far. In this paper we analyze by means of DFT calculations at the generalized gradient approximation level the bonding of pentalene in a series of real and hypothetical compounds of the type $[CpM(C_8H_6)]$, $[(CO)_3M(C_8H_6)]$, $[M(C_8H_6)_2]$, $[(CpM)_2(C_8H_6)]$, $[\{(CO)_3M\}_2(C_8H_6)]$, and $[M_2(C_8H_6)_2]$ (M = transition metal). Unless specified in the text, all the computed compounds have been characterized as minima on the potential energy hypersurface by vibrational frequency calculations (see Computational Details).

Results and Discussion

Electron counting formalism: The pentalene ligand is a potential 10-electron donor and is formally considered to be a dianion. However, the actual number of electrons given to a metal depends on the hapticity of pentalene and thus it is often lower than 10. Such a situation can also sometimes occur with the cyclopentadienyl monoanion, a potential six-electron donor. Thus, we will define two different electron counts for the studied compounds. 1) The total number of electrons (TNE), which is the sum of all the π electrons that can potentially be donated by the pentalene and/or cyclopentadiene anions, the metal valence electrons, and the terminal ligand electrons. For example, in the case of a $[(CO)_3M(C_8H_6)]$ system, $TNE = 10 + n + 3 \times 2$, where 10 is the total number of π electrons in the pentalene dianion and n is the number of valence electrons in M^{II}. Similarly, for a $[CpM(C_8H_6)]$ complex, $TNE = 10 + n' + 6$, where n' is the number of valence electrons in M^{III}. 2) The number of metal valence electrons (MVE), which corresponds to the number of electrons really belonging to the metallic sphere. This number depends on the hapticity of the pentalene and cyclopentadienyl ligands. It is clearly often equal or close to 18 and MVE is always less than or equal to TNE.

Free pentalene and the pentalene dianion: The molecular and electronic structures of pentalene and its dianion are well known.[1,2] Nevertheless we have optimized their geometries in order to compare their computed data with those of complexed pentalene species. They have C_{2h} and D_{2h} symmetry, respectively. Their optimized structures are shown in Figure 1 and the π-type MO diagram of $C_8H_6^{2-}$ is shown in Figure 2. The 10 π electrons lie in four bonding and one nonbonding MO. The latter is the HOMO π_5 which is located on the more electron-rich carbon atoms. Thus, these four atoms are privileged sites for metal complexation. The existence of three vacant antibonding MOs allows the possibility of π back-donation.

[CpM(pentalene)] and [(CO)$_3$M(pentalene)] complexes:
18 and 16 TNEs: We start our analysis with $[CpV(\eta^8\text{-}C_8H_6)]$ (TNE = 18), which was synthesized and structurally characterized by Jonas et al.[8a] and which we will use as a benchmark for our calculations. In this compound, all the pentalene carbon atoms are bonded to the metal. This suggests that pentalene donates all its π electrons to the metal, thus MVE = TNE = 18. The major computed data are given in Table 1 and the optimized structure and MO diagrams are shown in Figure 3 and Figure 4, respectively. The molecule has C_s symmetry. Taking into account the fact that this type of calculation usually overestimates the metal–ligand bond lengths by 2–5 % there is a good agreement between the optimized and experimental structures. In particular, the angle made by the two C_5 rings of the pentalene ligand is almost the same in both structures. The fragment analysis, which can be performed with the ADF program (see Computational Details),[16] allows the occupation of the π orbitals of the pentalene dianion after interaction with the CpV^{2+} moiety to be calculated. These values vary between

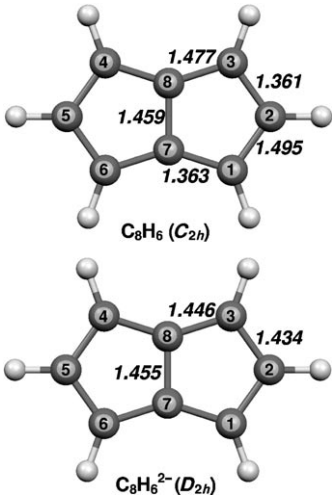

Figure 1. Optimized structures of neutral and dianionic pentalene. Interatomic distances are given in Å.

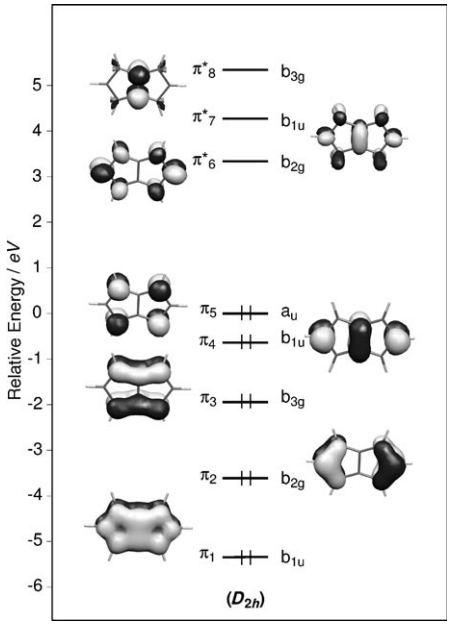

Figure 2. The π MO diagram of $C_8H_6^{2-}$.

Table 1. Computed data for 16- 18- and 20-TNE [CpM(C_8H_5R)] (R = H, ferrocenyl) and [$(CO)_3$M(C_8H_6)] model complexes. Averaged available experimental values[8a,18] are given in parentheses.

	[CpSc(C_8H_6)] C_s	[CpV(C_8H_6)] C_s	[CpMn(C_8H_6)] C_s ($S=1$)	[CpFe(C_8H_6)]$^+$ C_s	[CpFe($C_8H_4Fc_2$)]$^+$ C_s	[$(CO)_3$Cr(C_8H_6)] C_s
TNE	16	18	20	20	20	20
HOMO–LUMO gap [eV]	2.25	1.38	N/A	0.68	0.79	0.92
M−C7 [Å]	2.241	2.094 (2.051)	2.244	2.084	2.086 (2.026)	2.232
M−C1 [Å]	2.485	2.258 (2.209)	2.104	2.101	2.082 (2.036)	2.207
M−C2 [Å]	2.631	2.355 (2.312)	2.072	2.111	2.081(2.026)	2.223
M−C4 [Å]	2.485	2.274 (2.212)				
M−C5 [Å]	2.631	2.382 (2.308)				
δ [%][a]	−15	−11 (−11)	8	−1	0 (0)	0
M−C(Cp) or M−C(CO)						
average [Å]	2.529	2.272 (2.224)	2.210	2.130	2.115 (2.046)	1.883
range [Å]	2.515–2.545	2.210–2.315 (2.216–2.233)	2.171–2.238	2.105–2.150	2.103–2.125 (2.022–2.076)	1.863–1.924
C−C(pentalene)						
average [Å]	1.435	1.439 (1.413)	1.436	1.433	1.439 (1.430)	1.430
C1−C7 [Å]	1.443	1.445 (1.431)	1.442	1.440	1.438 (1.427)	1.434
C1−C2 [Å]	1.420	1.429 (1.394)	1.448	1.434	1.437 (1.416)	1.433
C6−C7 [Å]	1.443	1.445 (1.424)	1.419	1.440	1.465 (1.461)	1.434
C5−C6	1.420	1.427 (1.383)	1.416	1.409	1.414 (1.409)	1.410
C7−C8	1.465	1.463 (1.453)	1.473	1.449	1.443 (1.441)	1.449
C3-C8-C7-C6 [°]	149	137 (135)	175	177	179 (177)	178

[a] $\delta = [(M-C7)-(M-C2)]/(M-C2)$.

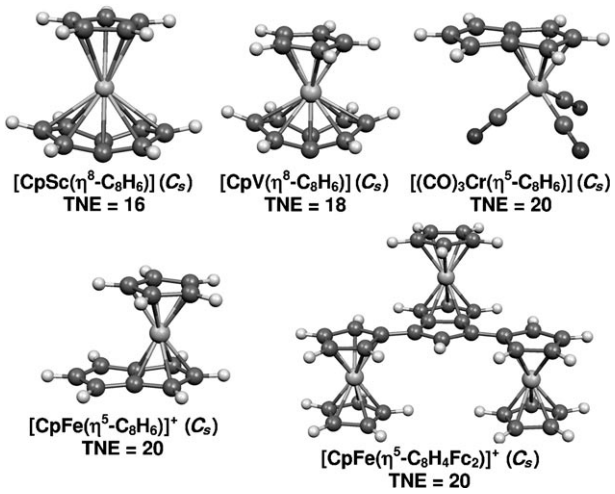

Figure 3. Optimized geometries of the 16-, 18-, and 20-TNE model complexes [CpM(C_8H_6)] (M = Sc, V, Fe), [CpFe($C_8H_4Fc)_2$]$^+$, and [$(CO)_3$Cr-(C_8H_6)].

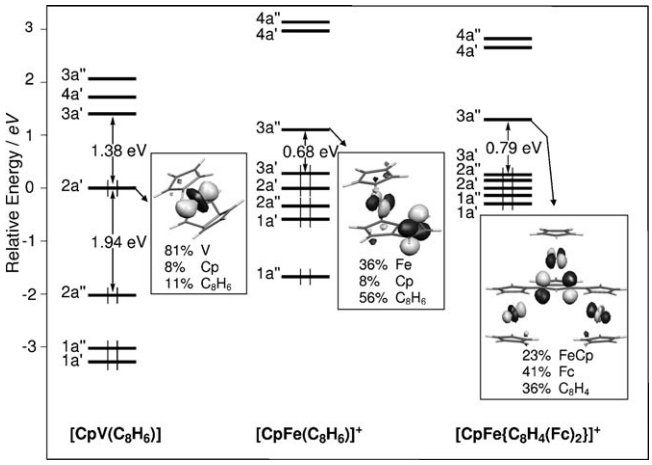

Figure 4. MO diagrams of [CpV(η^5-C_8H_6)], [CpFe(η^5-C_8H_6)]$^+$, and [CpFe(η^5-$C_8H_4Fc_2$)]$^+$.

1.81 (for π_1) and 1.25 (for π_5), indicating significant donation of all the occupied π orbitals to the metal. There is also significant back-donation to the vacant π_7^* orbital (occupation 0.26) which participates in a bonding way to the metallic HOMO. These data are fully consistent with the description of [CpV(η^8-C_8H_6)] as an 18-MVE V^{III} (d^2) complex.

The [CpV(η^8-C_8H_6)] HOMO is isolated in the middle of a large energy gap (Figure 4). This suggests the possibility of lower electron counts for the same structure type. Indeed, the 17-MVE [CpTi(η^8-C_8H_6)] complex has also been isolated[8] and related 16-NVE species are known, namely $Cl_3Ta[\eta^8$-$C_8H_4(SiMe_3)_2$-1,4][9a] and [Cp*U[η^8-$C_8H_4(Si\mathit{i}Pr_3)_2$-1,4] (Cp* = C_5Me_5).[9f] Consistent with this, optimization of the 16-TNE [CpSc(C_8H_6)] model leads to a similar structure (Figure 3) with a large HOMO–LUMO gap (Table 1). In this compound, the pentalene ligand is less folded than in the vanadium derivative as a result of the depopulation of the bonding Sc−C2,5 HOMO on going from V to Sc (see above). The folding angle of [CpSc(η^8-C_8H_6)] (149°) is close to that found experimentally for the isoelectronic complex $Cl_3Ta[\eta^8$-$C_8H_4(SiMe_3)_2$-1,4] (145°). It is likely that such 16-TNE/16-MVE species are more stable with heavier metals, the size of which allows a smaller relative difference between the longer Sc−C2,5 bonds and the shorter Sc−C7,8 ones.

20 TNEs: The η^8 coordination mode of pentalene cannot hold more than 18 TNE. In the optimized 20-TNE [CpFe-(C_8H_6)]$^+$ model, the metal is shifted to a quite symmetrical

η^5 coordination (see Table 1, Figure 3, and Figure 4). One may be tempted to describe this compound as an electron-deficient 16-MVE d^4 sandwich complex. Consistent with this view, it exhibits a low-lying LUMO with a rather small HOMO–LUMO gap of 0.68 eV (Figure 4) and its triplet state is computed to be less stable than the singlet ground state by only 0.24 eV. However, analysis of this LUMO reveals that this orbital, which should be largely metallic in character if $[CpFe(\eta^5\text{-}C_8H_6)]^+$ is a real 16-MVE complex (i.e. a member of the so-called "t_{2g}" set) is in fact largely delocalized on the C1 and C3 atoms. It has a large π_5(pentalene) character mixed in an out-of-phase way with a "t_{2g}" d-type AO. In other words, the electron deficiency is shared between these two carbon atoms and the metal. Consistent with this, the net charges on the C4 and C6 atoms are rather high (+0.27 compared with +0.12 and +0.18 for C7 and C5, respectively). Therefore, the bonding in this complex can be described by the canonical Lewis formulae shown in Scheme 2 with larger weights for the carbocationic forms **IIa** and **IIb**. Therefore, the pentalene ligand would be better

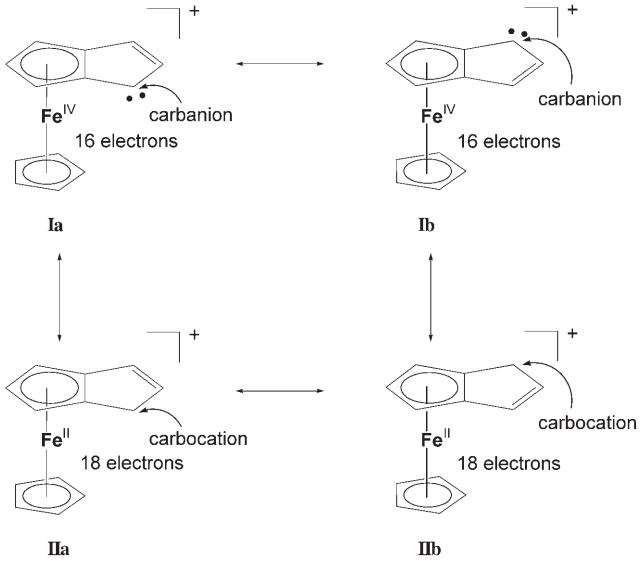

Scheme 2. The canonical Lewis formulae that can be used to describe the bonding in $[CpFe(\eta^5\text{-}C_8H_6)]^+$.

considered as formally being neutral and made of an aromatic C_5 ring linked to an allylic cation (**II**) rather than as an aromatic dianion (**I**). This allylium character should render the hypothetical $[CpFe(\eta^5\text{-}C_8H_6)]^+$ complex quite reactive. This is likely the reason why several complexes of hydropentalene (C_8H_7), which can formally be described as resulting from an hydride attack on the C4 or C6 atom of a 20-TNE $[CpM(\eta^5\text{-}C_8H_6)]$ complex, are known.[17] However, a compound related to $[CpFe(\eta^5\text{-}C_8H_6)]^+$ has been isolated and structurally characterized, namely $[CpFe(\eta^5\text{-}C_8H_4Fc_2)]^+$ (Fc = ferrocenyl).[18] In this compound the Fc units are bonded to the C4 and C6 atoms. Calculations revealed a larger HOMO–LUMO gap for this complex (0.79 eV) (Table 1, Figure 3, and Figure 4) than for $[CpFe(\eta^5\text{-}C_8H_6)]^+$ and significant delocalization of the LUMO on the Fc substituents. Although the LUMO plot (Figure 4) seems to support the authors' view[18] of through-space stabilization of the allylium system by the iron atoms of the Fc units, one should note that the corresponding Fe(Fc)···$C^{\delta+}$ distances are long (optimized: 3.12 Å; experimental: 2.94 Å). In fact, significant through-bond stabilization occurs via the Cp rings bonded to the $C^{\delta+}$ atoms. Clearly, the Fc units act as donor substituents which help to stabilize the allylium part of the molecule. Replacing the Fc units by NH_2 groups in the calculations resulted in a larger HOMO–LUMO gap (1.37 eV) and similar (25%) and larger (52%) FeCp and C_8H_4 LUMO participations, respectively.

Calculations on the isoelectronic models $[CpMn(\eta^5\text{-}C_8H_6)]$ and $[(CO)_3Cr(\eta^5\text{-}C_8H_6)]$ (Table 1 and Figure 3) yielded different results. The latter has a similar electronic structure to $[CpFe(\eta^5\text{-}C_8H_6)]^+$ with a larger HOMO–LUMO gap and LUMO participations of 31 and 52% for chromium and C_8H_4, respectively. The former was found to have a triplet ground state, the singlet state being 0.20 eV higher in energy. The instability of this singlet state originates from the large metal character (55%) of its low-lying LUMO.

These results indicate that 20-TNE complexes of the type $[L_3M(\eta^5\text{-pentalene})]$ are sufficiently stable to be isolated providing that 1) the L_3M group is sufficiently electron-withdrawing to induce significant allylium character into the uncomplexed side of pentalene and 2) this allylium moiety is electronically stabilized by electron-donating substituents on the C4 and C6 atoms.

22 TNEs: The addition of two electrons to $[CpFe(C_8H_6)]^+$ results in the loss of its electron deficiency. $[CpFe(C_8H_6)]^-$ has a similar structure to its related cation but with the projection of iron on the complexed pentalene η^5-C_5 ring somewhat shifted towards the C2 atom (Table 2, Figure 5). This shifting can be related to the so-called indenyl effect described in related indenyl complexes.[19c] The amount of shift can be evaluated from the relative difference between the shorter (Fe–C2) and longer (Fe–C7) bonds, that is, $\delta = [(Fe\text{–}C7)-(Fe\text{–}C2)]/(Fe\text{–}C2)$. In the case of $[CpFe(C_8H_6)]^-$, $\delta = 12\%$ (Table 2) compared with -1% for its related cation (Table 1). The HOMO–LUMO gap is large (1.68 eV) and the HOMO has a somewhat larger metal character (46%) and lower pentalene character (43%) than the LUMO of the cation. The net charges on the C4 and C6 atoms (+0.06 vs. +0.14 and +0.12 for the C7 and C5 atoms, respectively) do not reveal any strong carbanionic character. Thus, the calculations show that the uncomplexed part of pentalene does not have a strong allylide character. $[CpFe(C_8H_6)]^-$ is a d^6 18-MVE sandwich complex, isoelectronic with ferrocene, which should be stable enough to be isolated.

Geometry optimization of the isoelectronic compounds $[CpCo(C_8H_6)]$, $[CpNi(C_8H_6)]^+$, and $[(CO)_3Fe(C_8H_6)]$ showed a stronger metal shift towards the C2 atom (Table 2), especially in the two last models ($\delta = 18$–19%), which are best described as η^3-pentalene complexes. Thus,

Table 2. Computed data for 22-TNE $[CpM(C_8H_6)]$ and $[(CO)_3M(C_8H_6)]$ model complexes.

	$[CpFe(C_8H_6)]^-$ C_s	$[CpCo(C_8H_6)]$ C_s	$[CpNi(C_8H_6)]^+$ C_s	$[(CO)_3Fe(C_8H_6)]$ C_s
TNE	22	22	22	22
HOMO–LUMO gap [eV]	1.68	1.29	1.03	1.51
M–C7 [Å]	2.270	2.286	2.376	2.428
M–C1 [Å]	2.072	2.065	2.121	2.165
M–C2 [Å]	2.022	1.996	2.002	2.059
δ [%][a]	12	15	19	18
M–C(Cp) or M–C(CO)				
average [Å]	2.090	2.108	2.154	1.805
range [Å]	2.057–2.119	2.086–2.122	2.138–2.167	1.800–1.816
C–C(pentalene)				
average [Å]	1.439	1.434	1.432	1.432
C1–C7 [Å]	1.445	1.435	1.422	1.426
C1–C2 [Å]	1.450	1.446	1.449	1.448
C6–C7 [Å]	1.426	1.412	1.405	1.405
C5–C6 [Å]	1.418	1.417	1.420	1.417
C7–C8 [Å]	1.470	1.482	1.497	1.499
C3-C8-C7-C6 [°]	179	180	177	177

[a] $\delta = [(M–C7)–(M–C2)]/(M–C2)$.

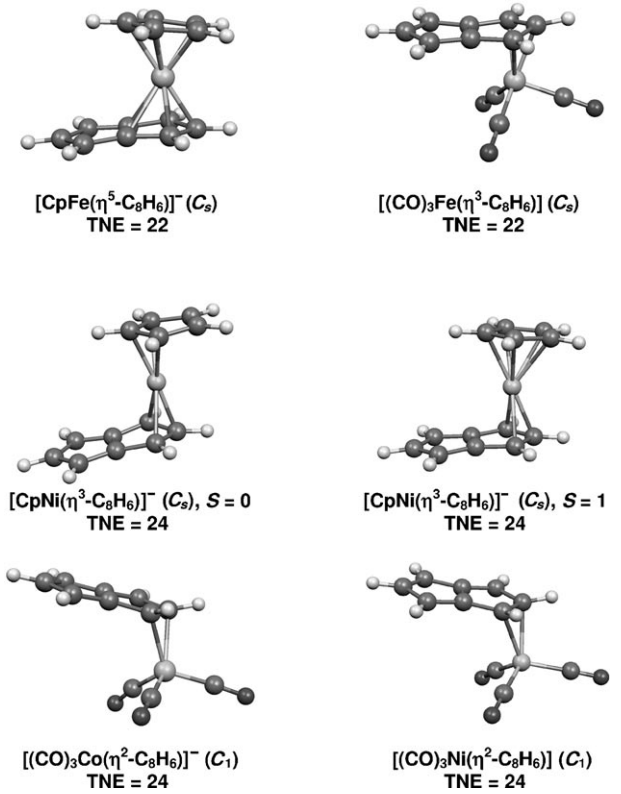

Figure 5. Optimized geometries of 22- and 24-TNE $[CpM(C_8H_6)]$ and $[(CO)_3M(C_8H_6)]$ model complexes.

$[(CO)_3Fe(C_8H_6)]$ can be viewed as a d^6 16-MVE complex of the pseudo-C_{4v} ML_5 type (Figure 5) in which the metal is bonded to the allylide part of a dianionic pentalene, the uncomplexed ring of which is aromatic. Consistent with this description, the LUMO of $[(CO)_3Fe(C_8H_6)]$ is an energy-isolated metal hybrid that points along the pseudo-C_4 axis. Thus, 22-TNE complexes of the type $[L_3M(C_8H_6)]$ can adopt either structure **a** or **b** of Scheme 3, or an intermediate form. The more electron-withdrawing the L_3M moiety, the more favored is structure **b**. Such compounds should be stable enough to be isolated.

Scheme 3. Two possible limiting structures (**a**,**b**) that can be adopted by 22-TNE complexes of the type $[L_3M(C_8H_6)]$.

24 TNEs: Partial ligand decoordination is anticipated on going from 22 to 24 TNE. This is what happens to both the pentalene and cyclopentadienyl ligands in the optimized geometry of $[(\eta^3\text{-Cp})Ni(\eta^3\text{-}C_8H_6)]^-$ in its singlet state (Table 3 and Figure 5). This model can be described as a d^8 16-MVE square-planar complex. The HOMO–LUMO gap is rather small (0.54 eV) and, consistent with this, there is a low-lying triplet state which lies only 0.07 eV above. In this triplet state the pentalene ligand is also η^3-bonded and the coordination mode of the Cp ligand is intermediate between η^5 and η^3. Interestingly, the pentalene moieties in the 24-TNE

Table 3. Computed data for 24-TNE $[CpM(C_8H_6)]$ and $[(CO)_3M(C_8H_6)]$ model complexes.

	$[CpNi(C_8H_6)]^-$ C_s $(S=0)$	C_s $(S=1)$	$[(CO)_3Co(C_8H_6)]^-$ C_1	$[(CO)_3Ni(C_8H_6)]$ C_1
TNE	24	24	24	24
HOMO–LUMO gap [eV]	0.54	–	1.11	1.31
M–C7 [Å]	2.754	2.541	3.117	3.147
M–C1 [Å]	2.173	2.237	2.191	2.261
M–C2 [Å]	1.969	2.068	2.136	2.205
δ [%][a]	40	23	–	–
M–C(Cp) or M–C(CO)				
average [Å]	2.341	2.287	1.794	1.857
range [Å]	2.070–2.595	2.230–2.329	1.781–1.809	1.847–1.868
C–C(pentalene)				
average [Å]	1.435	1.436	1.433	1.431
C1–C7 [Å]	1.452	1.437	1.476	1.472
C1–C2 [Å]	1.446	1.445	1.425	1.403
C6–C7 [Å]	1.419	1.422	1.376	1.366
C5–C6 [Å]	1.425	1.422	1.472	1.485
C7–C8 [Å]	1.434	1.470	1.461	1.458
C2–C3 [Å]			1.476	1.497
C3–C8 [Å]			1.374	1.362
C4–C8 [Å]			1.458	1.472
C4–C5 [Å]			1.378	1.365
C3-C8-C7-C6 [°]	176	180	178	180

[a] $\delta = [(M–C7)–(M–C2)]/(M–C2)$.

species $[(CO)_3Co(C_8H_6)]^-$ and $[(CO)_3Ni(C_8H_6)]$ exhibit an η^2 coordination mode, the coordinating bond being C1–C2. The resulting unsymmetrical geometry of $[(CO)_3Ni(C_8H_6)]$ and $[(CO)_3Co(C_8H_6)]^-$ is shown in Figure 5. The significant HOMO–LUMO gap computed for these species (Table 3) is at first surprising if one assumes a d^8 metal configuration (i.e. a dianionic pentalene ligand) for such a tetrahedral environment. It turns out that the π_5 orbital of pentalene is weakly populated in these complexes (0.23 electron in $[(CO)_3Ni(C_8H_6)]$), indicating a formal neutral oxidation state for this ligand. Consistent with this, the pentalene ligand exhibits C–C bond-length alternation as in free neutral pentalene (see Figure 1 and Table 3). Thus, these complexes should be viewed as d^{10} 18-MVE tetrahedral complexes. Unlike their cyclopentadienyl 24-TNE analogues they should be stable enough to be isolated.

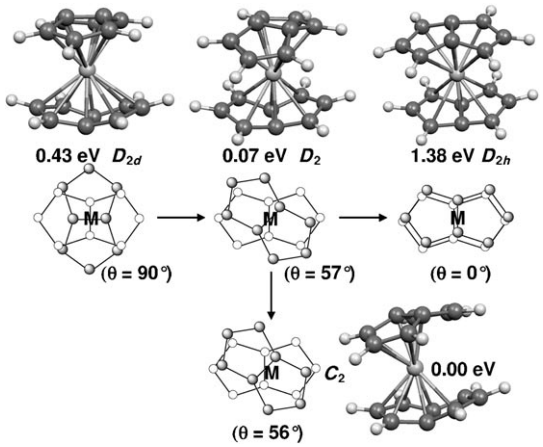

Figure 6. Structural relationships and relative energies computed for $[Ti(C_8H_6)_2]$ with D_{2d}, D_{2h}, D_2, and C_2 geometries. The D_{2h} conformation is a triplet state.

$[M(pentalene)_2]$ complexes:
20 and 18 TNEs: There is no crystal structure available for the 20-TNE complex $[Ti(C_8H_6)_2]$ made by Jonas et al.,[8b] who initially proposed the D_{2d} geometry shown in Figure 6. Previous calculations by our group on this complex assuming the D_{2d} conformation showed that this conformation corresponds to an 18-MVE d^0 system.[11b] Indeed, the a_2 out-of-phase combination of the pentalene π_5 orbitals cannot interact with the metal by symmetry (see the left side of Figure 7). Thus, as a whole the two pentalene dianions donate 18 electrons of the 20 they have available. However, more recent calculations by Jonas and co-workers[8d] on $[M(C_8H_6)_2]$ (M = Zr, Hf) showed a structure of D_2 symmetry, intermediate between the D_{2d} (staggered) and D_{2h} (eclipsed) conformations (see Figure 6) and with $\theta \approx 50°$. In the case of M = Ti, these authors found a C_1 geometry which can be viewed as a distorted D_2 conformation. Calculations on related $[M(\eta^8\text{-}C_8H_6)_2]$ (M = Th, U) complexes by Cloke et al. also showed a D_2-like geometry ($\theta = 49°$),[9d] which is in agreement with the crystal structure of a silyl-substituted thallium derivative.[9b] In the work reported here, frequency calculations showed that the D_{2d} conformation of $[Ti(\eta^8\text{-}C_8H_6)_2]$ is in fact a transition state between two D_2 conformations ($\theta = 57°$). The computed barrier is 0.36 eV. Further calculations revealed that the D_2 conformation is not an energy minimum. This minimum corresponds to a structure of C_2 symmetry which results from a distortion away from D_2 caused by a shift of the metal atom along one of the C_2 axes (Figure 6). However, the computed energy difference between the D_2 and C_2 conformations is very small (0.07 eV) indicating a flat potential energy surface around the minimum. Interestingly, $[Zr(\eta^5\text{-}C_8H_6)_2]$ was found to exhibit a D_2 conformation with $\theta = 55°$, in agreement with the work of Jonas and co-workers.[8d] Relevant computed data concerning $[Ti(C_8H_6)_2]$ and $[Zr(C_8H_6)_2]$ are given in Table 4.

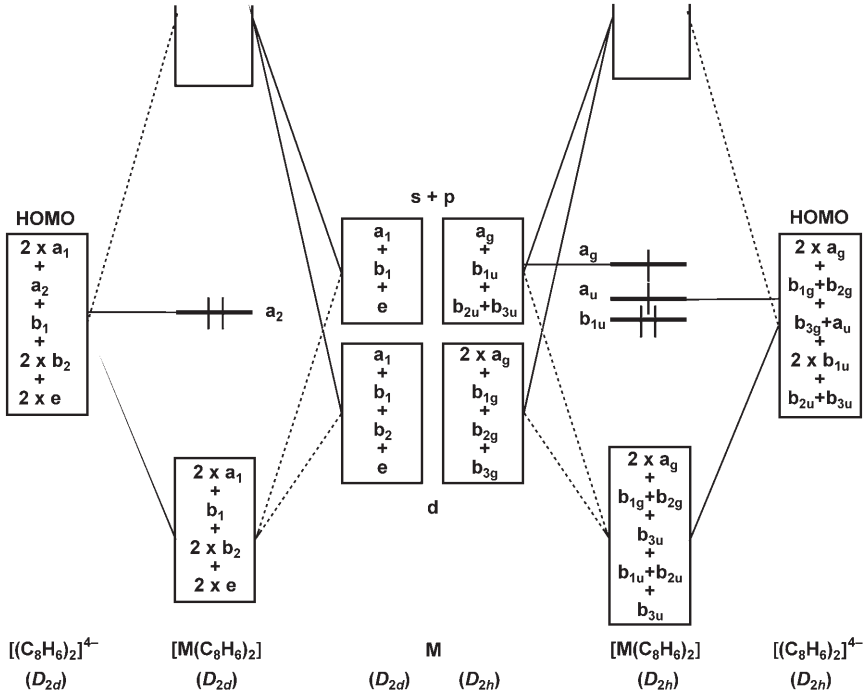

Figure 7. Qualitative MO diagram for a d^0 $[M(\eta^8\text{-}C_8H_6)_2]$ complex in the D_{2d} (left side) and D_{2h} (right side) conformations.

Being intermediate between the D_{2d} and D_{2h} geometries, the D_2 (or near D_2) conformation found for these 20-TNE

Table 4. Computed data for $[Ti(C_8H_6)_2]^{2+}$, $[Ti(C_8H_6)_2]$, and $[Zr(C_8H_6)_2]$.

	$[Ti(C_8H_6)_2]^{2+}$	$[Ti(C_8H_6)_2]$				$[Zr(C_8H_6)_2]$
	D_{2d}	D_{2d}	D_{2h} ($S=1$)	D_2	C_2	D_2
TNE	18	20	20	20	20	20
HOMO–LUMO gap [eV]	1.84	1.24	–	2.13	2.34	2.58
relative energy [eV]	–	0.43	1.38	0.07	0.00	–
M–C7 [Å]	2.190	2.193	2.259	2.205	2.187	2.353
M–C1 [Å]	2.459	2.470	2.527	2.492	2.324	2.601
M–C2 [Å]	2.580	2.583	2.697	2.617	2.471	2.731
M–C3 [Å]				2.417	2.412	2.559
M–C4 [Å]					2.717	
M–C5 [Å]					2.822	
M–C6 [Å]					2.460	
M–C8 [Å]					2.242	
C–C(pentalene)						
average [Å]	1.433	1.433	1.433	1.433	1.435	1.434
C1–C7 [Å]	1.433	1.433	1.441	1.447	1.444	1.449
C1–C2 [Å]	1.426	1.421	1.420	1.405	1.422	1.410
C7–C8 [Å]	1.458	1.481	1.450	1.460	1.460	1.460
C2–C3 [Å]				1.432	1.422	1.432
C3–C8 [Å]				1.435	1.436	1.434
C4–C8 [Å]					1.447	
C4–C5 [Å]					1.395	
C5–C6 [Å]					1.442	
C6–C7 [Å]					1.443	
C3-C8-C7-C6 [°]	150	151	152	152	155	152

species is surprising with respect to electron counting. Indeed, from symmetry arguments the D_{2d} conformation satisfies the 18-electron rule and therefore is expected to have the strongest metal–ligand bonds (Figure 7, left). On the other hand, the same considerations lead to predictions that the D_{2h} conformation is an unstable 16-electron system with an expected small HOMO–LUMO gap (Figure 7, right).

Consistent with this, this conformation (right side of Figure 6) was computed to be a triplet state. The reason for the $D_{2d} \rightarrow D_2$ distortion lies in the ligand–ligand through-space antibonding character of the D_{2d} a_2 HOMO. Being an antibonding combination of two pentalene π_5 orbitals, this MO is localized on the C1,3,4,6 atoms (see Figure 1 labels). It follows that the interligand repulsion is maximized in the D_{2d} conformation in which these atoms are eclipsed.[8d] A rotation of $\theta \approx 45°$ minimizes this repulsion. Thus, the D_2 conformation adopted by $[Zr(C_8H_6)_2]$ is the result of a compromise between metal–ligand bonding and ligand–ligand repulsion. The fact that $[Ti(C_8H_6)_2]$ is found to be slightly more stable in the C_2 conformation is likely due to the smaller size of titanium which has difficulty in bonding similarly to 16 carbon atoms at the same time.

In the D_{2d} conformation, the HOMO of $[M(C_8H_6)_2]$ (M = Ti, Zr) is isolated in the middle of a large energy gap (Figure 7, left). This suggests the possibility of lower electron counts for the same structure.[11b] Its depopulation would not change the MVE count since this orbital is ligand-based. Moreover in the D_{2d} conformation this depopulation would change the interligand repulsion into an attraction. In fact, the $[Ti(\eta^8\text{-}C_8H_6)_2]^{2+}$ ion was computed to adopt the D_{2d} conformation. Its major computed data are given in Table 4. Such d^0 18-TNE/18-MVE cations might be isolable, especially with heavier Group 3 metals.

22, 24, and 26 TNEs: Calculations on the $[M(C_8H_6)_2]$ (M = Cr, Fe, Ni) models provided results fully consistent with those obtained for the cyclopentadienyl series (Table 5 and Figure 8). With M = Cr, the optimized structure is of the type $[(\eta^5\text{-}C_8H_6)M(\eta^8\text{-}C_8H_6)]$. This is a 22-TNE/18-MVE complex of Cr^{IV}, isoelectronic with $[CpV(\eta^8\text{-}C_8H_6)]$, with one pentalene dianion acting as a ten-electron donor and the other one as a six-electron donor. This latter pentalene dianion does not exhibit significant allylide character on its uncomplexed part. Such a compound has not been isolated so far, but related isoelectronic substituted indenyl complexes of the type $[(\eta^5\text{-indenyl})Zr(\eta^9\text{-indenyl})]$ have been characterized[20a] and their electronic structure recently investigated.[20b]

The compound corresponding to M = Fe was isolated[4d] and structurally characterized[21] a long time ago. This C_2-symmetric molecule has an inter-pentalene bond of 1.568(7) Å. Its bonding can formally be described as being the result of the dimerization of two pentalene radical monoanions and their complexation by a Fe^{II} cation, as shown in Scheme 4. Thus, C_2 $[Fe(C_8H_6)_2]$ is a ferrocene derivative (18 MVEs). Two conformations can be proposed, depending on which side of the allylic radical is involved in the dimerization. In agreement with experiment, the C_2 isomer was found to be more stable than the C_s isomer, which is more constrained (Table 5 and Figure 8). This is exemplified by the longer inter-pentalene bond in the C_s isomer (1.617 versus 1.592 Å). These isomers should be considered as 22-TNE species since the electron pair associated with the inter-pentalene bond should not be included in the TNE count (see Electron counting formalism section). Interestingly, we found another isomer, of C_{2v} symmetry (Figure 8), which is derived from the C_s isomer by breaking the inter-pentalene bond and which is less stable by only 0.07 eV (Table 5). It has a singlet ground state. Surprisingly, it is 0.70 eV more stable in this face-to-face C_{2v} geometry than in the C_{2h} one in which the uncomplexed rings are not eclipsed. Such behavior has also been shown to exist in bis-indenyl complexes.[19] If one assumes that in this $[Fe(\eta^5\text{-}C_8H_6)_2]$ C_{2v} structure the pentalene ligands are formally dianions, one is left with a 16-MVE electron-deficient structure. Examination of the LUMO (Figure 9) shows that, as in the case of $[CpFe(\eta^5\text{-}C_8H_6)]^+$, the electron deficiency is shared between the iron atom and the ligands. In the bis-pentalene complex, however, this deficiency is delocalized onto both ligands, that is, onto four carbon atoms. The triplet state is found to be 0.10 eV higher in energy than the singlet state and adopts the C_{2h} conformation. Such a 24-TNE species is likely to be very reactive. This is probably the reason why only bis-hydropentalenyl complexes have been isolated so far.[17] However, they might be isolable if they bear protect-

Table 5. Computed data for 22-, 24-, and 26-TNE $[M(C_8H_6)_2]$ model complexes. Averaged available experimental values[21] are given in parentheses.

	$[Cr(C_8H_6)_2]$		$[Fe(C_8H_6)_2]$			$[Ni(C_8H_6)_2]$
	C_s	C_{2v}	C_{2h} ($S=1$)	C_s	C_2	C_{2v}
TNE	22	24	24	22[a]	22[a]	26
HOMO–LUMO gap [eV]	1.35	0.72	–	1.93	2.12	0.70
relative energy [eV]	–	0.46	0.56	0.39	0.00	0.00
M–C7 [Å]	2.054	2.202	2.180	2.146	2.087 (2.049)	2.327
M–C1 [Å]	2.247	2.085	2.105	2.169	2.128 (2.082)	2.127
M–C2 [Å]	2.330	2.063	2.074	2.106	2.111 (2.066)	2.022
M–C3 [Å]	2.202			2.044	2.062 (2.016)	
M–C8 [Å]	2.036			1.998	2.008 (1.979)	
M–C7′ [Å]	2.396					
M–C1′ [Å]	2.174					
M–C2′ [Å]	2.124					
δ [%][b]	13	7	5	–	–	15
C–C(pentalene)						
average [Å]	1.440	1.432	1.434	1.454	1.453 (1.439)	1.434
C1–C7 [Å]	1.440	1.440	1.438	1.433	1.436 (1.423)	1.427
C1–C2 [Å]	1.422	1.438	1.440	1.440	1.441 (1.420)	1.449
C7–C8 [Å]	1.471	1.460	1.455	1.442	1.443 (1.414)	1.492
C2–C3 [Å]	1.432			1.446	1.446 (1.432)	
C3–C8 [Å]	1.442			1.436	1.437 (1.423)	
C4–C8 [Å]		1.425	1.436	1.535	1.537 (1.534)	1.410
C4–C5 [Å]		1.413	1.412	1.537	1.524 (1.509)	1.419
C5–C6 [Å]				1.358	1.355 (1.326)	
C6–C7 [Å]				1.457	1.465 (1.469)	
C1′–C7′ [Å]	1.439					
C1′–C2′ [Å]	1.444					
C7′–C8′ [Å]	1.468					
C4′–C8′ [Å]	1.414					
C4′–C5′ [Å]	1.417					
C4–C4′ [Å]				1.617	1.592 (1.568)	
C3-C8-C7-C6 [°]	136	180	179	167	178	179

[a] The electron pair associated with the inter-pentalene bond is not included in the TNE count (see text). [b] $\delta=[(M–C7)–(M–C2)]/(M–C2)$.

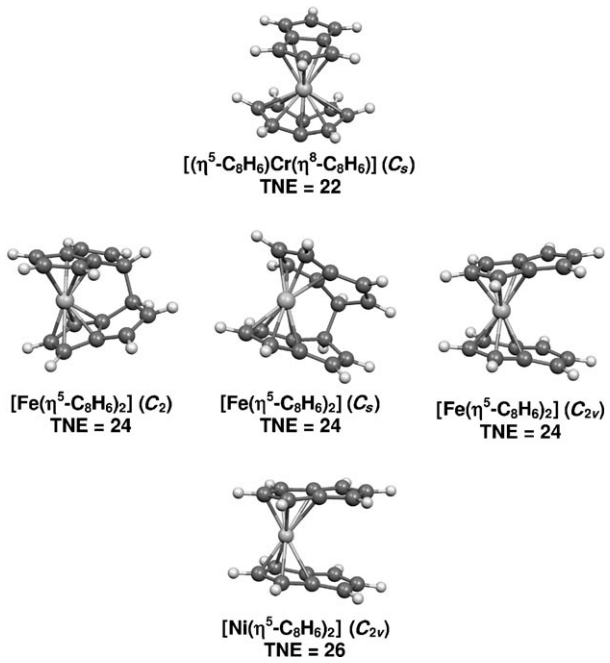

Figure 8. Optimized geometries of 22-, 24-, and 26-TNE $[M(C_8H_6)_2]$ model complexes [the electron pair associated with the inter-pentalene bond in C_2 and C_s $[Fe(C_8H_6)_2]$ is not included in the TNE count (see text)].

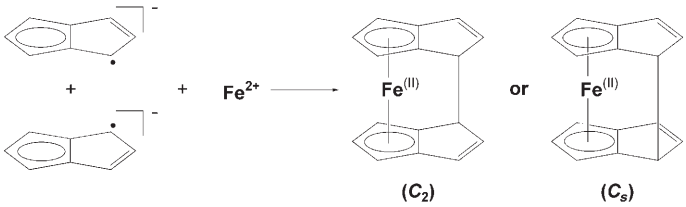

Scheme 4. The two conformations (C_2 and C_s) for the structure of $[Fe(C_8H_6)_2]$, which result formally from the dimerization of two pentalene radical monoanions and their complexation by a Fe^{II} cation.

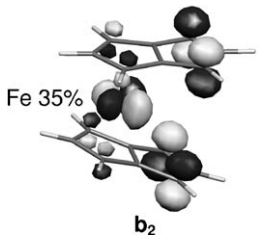

Figure 9. The LUMO of the $[Fe(\eta^5\text{-}C_8H_6)_2]$ C_{2v} isomer.

ing groups, as in the case of the related 20-TNE $[CpFe(C_8H_4Fc_2)]^+$ complex (see above).[18]

With M = Ni, the optimized structure is also a closed-shell configuration of the type $[Ni(\eta^5\text{-}C_8H_6)_2]$ with C_{2v} symmetry.

The C_{2h} conformation is found to be less stable by 0.13 eV. This is an 18-MVE species isoelectronic with [CpCo(η^5-C_8H_6)]. Its relatively small HOMO–LUMO gap is consistent with a low-lying triplet state, computed to be 0.49 eV higher in energy and which adopts the C_{2h} conformation.

[(CpM)$_2$(pentalene)] and [{(CO)$_3$M}$_2$(pentalene)] complexes: There are more examples of structurally characterized pentalene dinuclear complexes than of mononuclear complexes.[3] When both pentalene rings are complexed, the metal atoms can lie either on the same side of the ligand (*syn* configuration) or on opposite sides (*anti* configuration). The *syn* configuration is sterically more crowded but allows the possibility of metal–metal bonding (Scheme 5).[10b] We start our analysis with 34-TNE complexes, of which stable examples are known[6g,7a,c,10a] and which will serve as a reference for other electron counts.

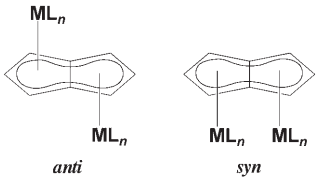

Scheme 5. The *anti* and *syn* configurations of pentalene dinuclear complexes.

34 TNEs: *anti*-[(Cp*Fe)$_2$(η^5,η^5-C_8H_6)] has been known for a long time.[7a,c] More recently, the isoelectronic species [{(CO)$_3$M}$_2$(η^5,η^5-C_8H_6)] (M = Mn, Re) has been characterized.[10a] While the manganese derivative has been shown to adopt the *anti* configuration in the solid state, the rhenium one crystallizes in both the *anti* and *syn* configurations. There is another example of a *syn* isomer, namely [{(CO)$_2$(GeMe)Ru}$_2$(η^5,η^5-C_8H_6)],[6g] whose *anti* counterpart is not known.

Geometry optimizations have been carried out for [(CpFe)$_2$(C_8H_6)] and [{(CO)$_3$M}$_2$(C_8H_6)] (M = Mn, Re) in both the *anti* and *syn* configurations. They are of C_{2h} and C_{2v} symmetry, respectively. The major computed data are given in Table 6. Note that the computed data are in rather good agreement with the available experimental data. The optimized structures of the *syn* and *anti* isomers of [(CpFe)$_2$(C_8H_6)] and [{(CO)$_3$Mn}$_2$(C_8H_6)] are shown in Figure 10. The analysis of the *anti*-[(CpFe)$_2$(C_8H_6)] MO diagram, based on the interaction between the frontier orbitals of $C_8H_6^{2-}$ and the $(CpFe\cdots FeCp)^{2+}$ fragment, has been reported else-

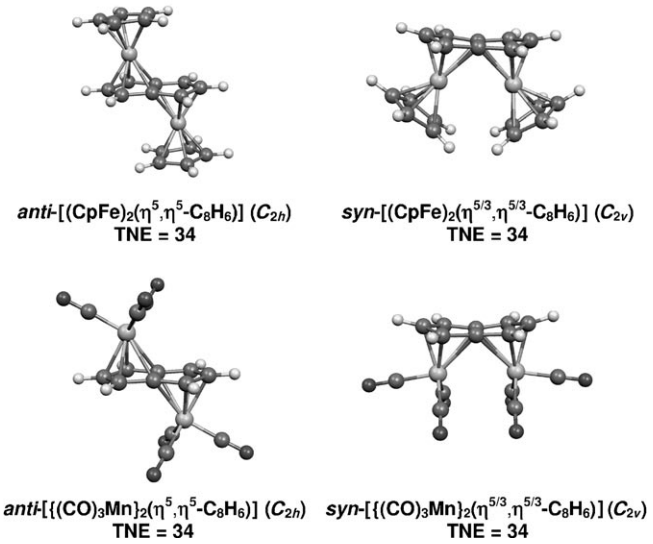

Figure 10. Optimized geometries of 34-TNE [(CpM)$_2$(C_8H_6)] and [{(CO)$_3$M}$_2$(C_8H_6)] complexes ($\eta^{5/3}$ indicates an hapticity intermediate between η^5 and η^3).

Table 6. Major computed data for the *syn* and *anti* isomers of [(CpFe)$_2$(C_8H_6)], [{(CO)$_3$Mn}$_2$(C_8H_6)], and [{(CO)$_3$Re}$_2$(C_8H_6)]. Averaged available experimental values[7a,c,10a] are given in parentheses.

	[(CpFe)$_2$(C_8H_6)]		[{(CO)$_3$Mn}$_2$(C_8H_6)]		[{(CO)$_3$Re}$_2$(C_8H_6)]	
	syn C_{2v}	*anti* C_{2h}	*syn* C_{2v}	*anti* C_{2h}	*syn* C_{2v}	*anti* C_{2h}
TNE	34	34	34	34	34	34
HOMO–LUMO gap [eV]	1.14	1.34	2.88	2.32	3.50	2.83
relative energy [eV]	0.53	0	0.24	0	0.02	0
M–C7 [Å]	2.401	2.165 (2.120)	2.503	2.311 (2.222)	2.655 (2.483)	2.488
M–C1 [Å]	2.098	2.062 (2.025)	2.200	2.186 (2.137)	2.341 (2.318)	2.335
M–C2 [Å]	2.006	2.051 (2.016)	2.104	2.158 (2.119)	2.234 (2.226)	2.290
δ [%][a]	20	6 (5)	19	7 (5)	19 (12)	9
M–C(Cp) or M–C(CO)						
average [Å]	2.088	2.089 (2.058)	1.812	1.813 (1.801)	1.932 (1.915)	1.929
range [Å]	2.072–2.116	2.081–2.091 (2.019–2.131)	1.783–1.827	1.782–1.794 (1.782–1.813)	1.907–1.945 (1.889–1.934)	1.906–1.904
C–C(pentalene)						
average [Å]	1.445	1.450 (1.428)	1.440	1.442 (1.438)	1.443 (1.431)	1.447
C1–C7 [Å]	1.440	1.447 (1.432)	1.440	1.447 (1.443)	1.440 (1.436)	1.453
C1–C2 [Å]	1.445	1.443 (1.414)	1.437	1.431 (1.425)	1.442 (1.424)	1.436
C7–C8 [Å]	1.463	1.497 (1.463)	1.455	1.446 (1.466)	1.462 (1.453)	1.469
M–M [Å]	3.180	–	3.273	–	3.390 (3.230)	–
C3-C8-C7-C6 [°]	173	180 (180)	172	180 (180)	173 (172)	180

[a] δ = [(M–C7) – (M–C2)]/(M–C2).

where.[11a] This MO diagram is sketched on the left side of Figure 11. Let us recall that the five occupied π-type $C_8H_6^{2-}$ orbitals interact in a bonding way with five of the six combi-

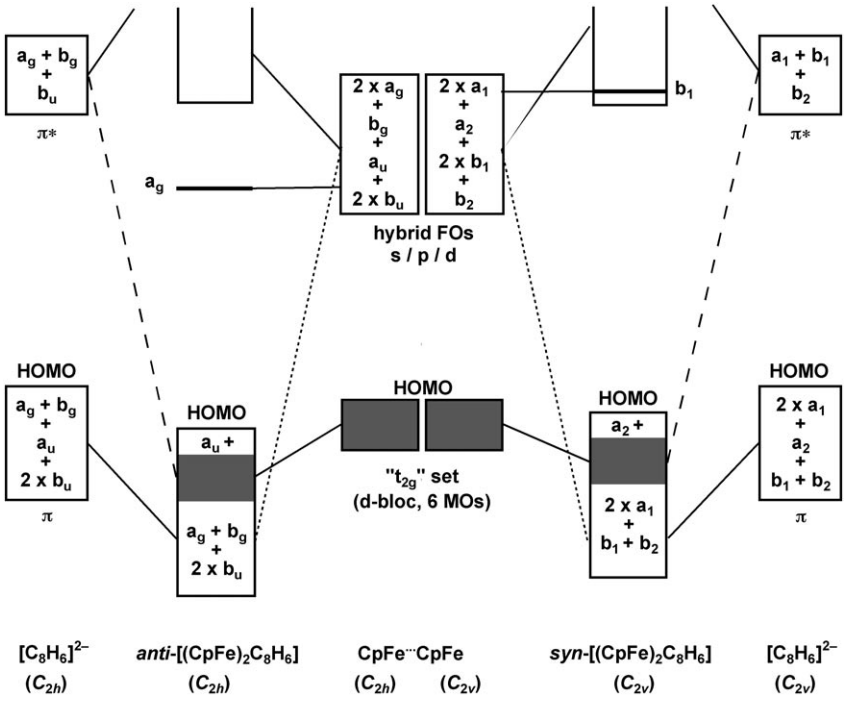

Figure 11. Qualitative MO diagram for the *anti* (left side) and *syn* (right side) configurations of $[(CpFe)_2(\eta^5\text{-}C_8H_6)]$.

nations of the vacant $[CpFe]^+$ hybrids. The sixth hybrid, of a_g symmetry, remains largely nonbonding and lies in the middle of a large energy gap. The 18-electron rule requires the occupation of this metallic nonbonding orbital.[19] However, its occupation is forbidden by its high energy (hybrid character). As a consequence *anti*-$[(CpFe)_2(\eta^5,\eta^5\text{-}C_8H_6)]$ is deficient by two electrons. As the deficiency is equally delocalized on both metals, they have to be considered as 18-/16-MVE (not 17-MVE) centers, as illustrated by the canonical Lewis formulae shown in Scheme 6. The shift of the iron atom towards the C2 atom is small ($\delta = 6\,\%$), indicative of a quite symmetrical η^5 coordination mode for both rings.

The qualitative interaction MO diagram of *syn*-$[(CpFe)_2(C_8H_6)]$ is quite similar to that of its *anti* counterpart

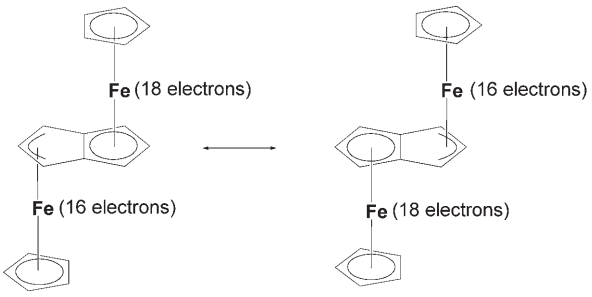

Scheme 6. The canonical Lewis formulae for *anti*-$[(CpFe)_2(\eta^5,\eta^5\text{-}C_8H_6)]$.

(Figure 11). However, some differences became apparent from the calculations. The b_1 LUMO has σ*(Fe–Fe) character and is higher in energy than the a_g LUMO of the *anti* isomer. More importantly, the steric repulsion between the Cp ligands is large such that the Cp ligands are not parallel to the pentalene plane and the iron atoms are significantly shifted towards the C2 atoms ($\delta = 20\,\%$), the pentalene coordination approaching the η^3 type. As a result, the *syn* configuration is less stable than the *anti* one by 0.53 eV.

The *anti*- and *syn*-$[\{(CO)_3M\}_2(C_8H_6)]$ (M = Mn, Re) series are electronically related to the $[(CpFe)_2(C_8H_6)]$ species. There are however some differences. The $[M(CO)_3]$ units are less bulky and more flexible than the Cp ligands. In the *syn* configurations they rotate away from the "vertical" axes in such a way that they can avoid each other. Consequently, in the case of M = Re, both conformers are almost isoenergetic (Table 6), in agreement with the experimental observations.[10a] In the case of M = Mn, the *syn* isomer is less stable by 0.24 eV, a value which does not exclude the possibility of isolating it, although only the *anti* species has been isolated so far.[10a] Note that, whereas the *anti* species exhibit moderate shifting of M towards the C2 atom ($\delta = 7$–$9\,\%$), the optimized *syn* isomers exhibit a strong distortion towards η^3 coordination ($\delta = 19\,\%$). This distortion is overestimated at least in the M = Re case, for which $\delta_{exp} = 12\,\%$. Nevertheless, this tendency for d^6 $M(CO)_3$ units to distort towards η^3 coordination to yield deficient 16-MVE ML_5-type systems is reminiscent of the 22-TNE $[(CO)_3Fe(C_8H_6)]$ model complex (see above). Also note that there is no evidence for metal–metal bonding in the *syn* species from the calculations (Table 6) nor from the X-ray structure of $[\{(CO)_3Re\}_2(\eta^5,\eta^5\text{-}C_8H_6)]$, where Re–Re = 3.23 Å.[10a] The situation is less straightforward for *syn*-$[\{(CO)_2(GeMe)Ru\}_2(\eta^5,\eta^5\text{-}C_8H_6)]$. The X-ray structure of this complex shows Ru–Ru = 3.06 Å.[6g] The corresponding optimized distance for this compound is, as expected, larger (3.25 Å). If any, the metal–metal bonding is weak and likely to originate from a through-bond interaction by mixing of the vacant b_1 σ*(Fe–Fe) MO (Figure 9, right) into occupied orbitals of the same character.

36, 38, and 40 TNEs: The 36- and 38-TNE *anti*-$[(Cp^*M)_2(C_8H_6)]$ (M = Co, Ni) complexes have been isolated and the

X-ray structure of the former is known.[7c] Geometry optimizations have been carried out on the related *anti*-$[\{(CO)_3M\}_2(C_8H_6)]$ (M = Co, Ni) models. Their optimized structures are shown in Figure 12 and relevant computed data are given in Table 7. Both models were found to have a singlet ground state, in agreement with the experimental data reported for related Cp* complexes.[7c] However, whereas the triplet state lies 0.32 eV above the singlet state in the case of M = Co, it is found to be only 0.04 eV less stable than the singlet state of the complex with M = Ni. The computed data available in the case of M = Co are in satisfactory agreement with the available experimental data. As already noted above, the shift towards η^3 coordination is overestimated in the optimized structure of *anti*-$[(CpCo)_2(C_8H_6)]$ ($\delta = 19\%$ versus $\delta_{exp} = 16\%$). The shift increases on going from Co to Ni, the latter clearly being coordinated in an η^3 fashion. Thus, *anti*-$[(CpNi)_2(\eta^3,\eta^3\text{-}C_8H_6)]$ (38-TNE) is an 18-/18-MVE species.

The 36- and 38-TNE $[\{(CO)_3M\}_2(C_8H_6)]$ (M = Fe, Co) models have been calculated in both the *syn* and *anti* configurations. The *anti* conformer was found to be more stable than the *syn* one by 0.78 and 0.29 eV for M = Fe and Co, respectively. We discuss here only the results corresponding to the more stable *anti* conformers for which relevant data and optimized structures are reported in Table 7 and Figure 12. *anti*-$[\{(CO)_3M\}_2(C_8H_6)]$ (M = Fe, Co) species exhibit similar shifting of the metal towards the C2 atoms as their isoelectronic metal–cyclopentadienyl relatives. $[\{(CO)_3Fe\}_2(C_8H_6)]$ exhibits a coordination mode intermediate between η^5 and η^3 ($\delta = 22\%$) and $[\{(CO)_3Co\}_2(C_8H_6)]$ is clearly η^3-coordinated ($\delta = 33\%$), that is, an 18-/18-MVE species.

In the 40-TNE $[\{(CO)_3Ni\}_2(C_8H_6)]$ model, the metal atoms were found to be η^2-coordinated, both in the *syn* and *anti* configurations (Figure 12). The *anti* isomer was found to be more stable than the *syn* one by only 0.06 eV. Only the data corresponding to the *anti* isomer are reported in Table 7. As in the case of $[(CO)_3Ni(\eta^2\text{-}C_8H_6)]$, the bonding in this species should be regarded as being a result of the coordination of neutral pentalene to 18-MVE Ni(0) metal centers.

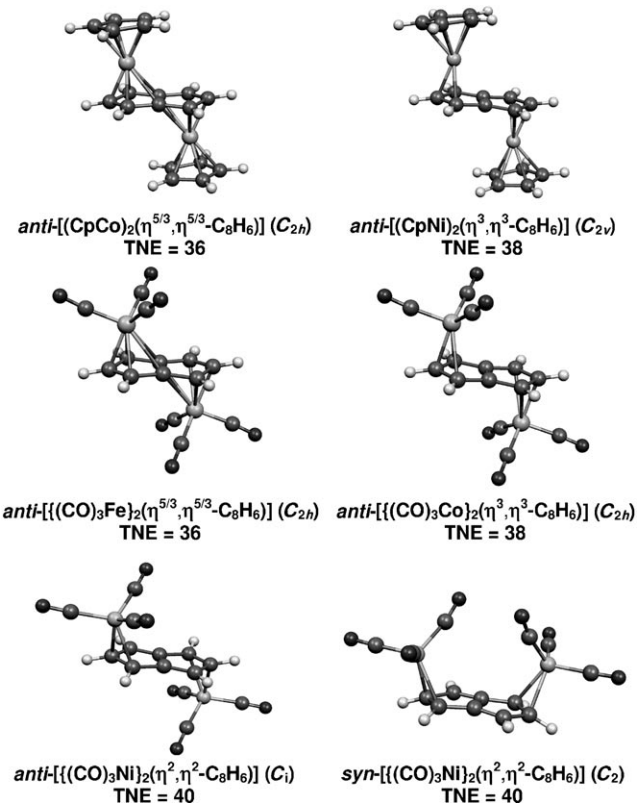

Figure 12. Optimized geometries of 36- to 40-TNE $[(CpM)_2(C_8H_6)]$ and $[\{(CO)_3M\}_2(C_8H_6)]$ complexes ($\eta^{5/3}$ indicates an hapticity intermediate between η^5 and η^3).

Table 7. Major computed data for *anti* isomers of $[(CpCo)_2(C_8H_6)]$, $[(CpNi)_2(C_8H_6)]$, $[\{(CO)_3Fe\}_2(C_8H_6)]$, $[\{(CO)_3Co\}_2(C_8H_6)]$, and $[\{(CO)_3Ni\}_2(C_8H_6)]$. Averaged available experimental values[7c] are given in parentheses.

	$[(CpCo)_2(C_8H_6)]$ C_{2h}	$[(CpNi)_2(C_8H_6)]$ C_{2h}	$[\{(CO)_3Fe\}_2(C_8H_6)]$ C_{2h}	$[\{(CO)_3Co\}_2(C_8H_6)]$ C_{2h}	$[\{(CO)_3Ni\}_2(C_8H_6)]$ C_i
TNE	36	38	36	38	40
HOMO–LUMO gap [eV]	0.82	0.37	1.11	0.58	1.45
M–C7 [Å]	2.369 (2.284)	2.558	2.535	2.806	3.148
M–C1 [Å]	2.085 (2.048)	2.194	2.194	2.379	2.283
M–C2 [Å]	1.989 (1.977)	1.985	2.078	2.106	2.252
δ [%][a]	19 (16)	29	22	33	–
M–C(Cp) or M–C(CO)					
average [Å]	2.128 (2.068)	2.209	1.802	1.826	1.853
range [Å]	2.115–2.170 (2.039–2.117)	2.193–2.223	1.793–1.820	1.798–1.840	1.847–1.864
C–C(pentalene)					
average [Å]	1.444 (1.426)	1.440	1.440	1.434	1.434
C1–C7 [Å]	1.443 (1.430)	1.420	1.442	1.410	1.472
C1–C2 [Å]	1.446 (1.422)	1.448	1.438	1.443	1.402
C7–C8 [Å]	1.443 (1.430)	1.486	1.440	1.496	1.460
C2–C3 [Å]					1.486
C3–C8 [Å]					1.365
C3-C8-C7-C6 [°]	180 (180)	180	180	180	180

[a] $\delta = [(M–C7)–(M–C2)]/(M–C2)$.

32, 30, and 28 TNEs: The removal of electrons from a stable 34-TNE species (Figure 11) induces unsaturation which can be released by the formation of metal–metal bonds. This can only be achieved in the *syn* configuration. The only example of this type so far characterized is the 28-TNE complex *syn*-$[(CpV)_2(\eta^5,\eta^5\text{-}C_8H_6)]$, which exhibits antiferromagnetic behavior and in which V–V = 2.54 Å.[10b] DFT calculations by the same authors are consistent with the existence of a triple bond in the low-spin state.[10b] We have performed calculations on the *syn*-$[(CpM)_2(C_8H_6)]$ (M = Mn, Cr, V) series which have 32, 30, and 28 TNEs, respectively. Their optimized structures, of C_{2v} symmetry, are shown in Figure 13. Relevant computed data are given in Table 8. Starting with the MO diagram of a *syn* 34-TNE species (right side of Figure 11), lowering the electron count corresponds to the depopulation of some of its d-block orbitals. These d-block orbitals are composed of in-phase and out-of-phase combinations of the so-called "t_{2g}" orbitals of the MCp units[22] which have approximate σ, $\pi_\perp$, and δ M–M character, respectively, if one assumes that the MCp C_5 axis remains perpendicular to the pentalene plane. These six combinations are sketched in Scheme 7. For simplicity we assume first that the Cp rings are parallel to the pentalene plane, an extreme situation which neglects steric hindrance. Note that the C_{2v} symmetry allows σ–δ and σ–δ mixing. When TNE < 34, bonds will be created if antibonding combinations are

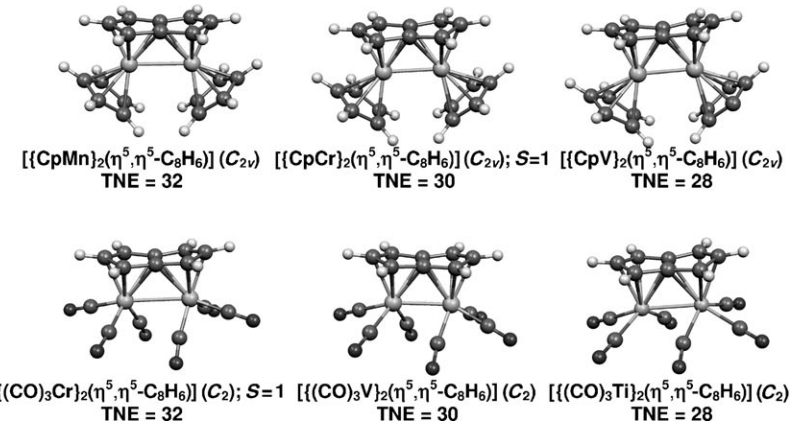

Figure 13. Optimized geometries of *syn*-$[(CpM)_2(C_8H_6)]$ (M = Mn, Cr, V) and *syn*-$[\{(CO)_3M\}_2(C_8H_6)]$ (M = Cr, V, Ti) in their lowest spin states.

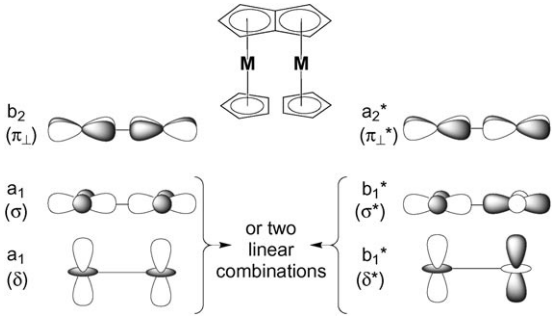

Scheme 7. The in-phase (left) and out-of-phase (right) combinations of "t_{2g}" orbitals of the MCp units in *syn*-$[(CpM)_2(C_8H_6)]$, assuming that the Cp ligands are parallel to the pentalene plane.

Table 8. Major computed data for *syn*-$[(CpM)_2(C_8H_6)]$ (M = Mn, Cr, V) and *syn*-$[\{(CO)_3M\}_2(C_8H_6)]$ (M = Ti, V, Cr). Averaged available experimental values[10b] are given in parentheses.

	$[(CpMn)_2(C_8H_6)]$ C_{2v}	$[(CpCr)_2(C_8H_6)]$ C_{2v} ($S=1$)	$[(CpV)_2(C_8H_6)]$ C_{2v} ($S=1$)	$[\{(CO)_3Cr\}_2(C_8H_6)]$ C_2 ($S=1$)	$[\{(CO)_3V\}_2(C_8H_6)]$ C_2	$[\{(CO)_3Ti\}_2(C_8H_6)]$ C_2
TNE	32	30	28	32	30	28
HOMO–LUMO gap [eV]	0.52				0.99	0.53
M–C7 [Å]	2.327	2.318	2.310 (2.305)	2.414	2.385	2.495
M–C1 [Å]	2.122	2.185	2.244 (2.221)	2.225	2.240	2.344
M–C2 [Å]	2.058	2.180	2.281 (2.236)	2.201	2.284	2.348
M–C3 [Å]				2.275	2.338	2.373
M–C8 [Å]				2.467	2.427	2.486
δ [%][a]	13	6	3 (3)			
M–C(Cp) or M–C(O)						
average [Å]	2.183	2.272	2.340 (2.276)	1.885	1.961	2.098
range [Å]	2.133–2.233	2.249–2.296	2.340–2.341 (2.272–2.296)	1.890–1.902	1.948–1.971	2.071–2.122
C–C(pentalene)						
average [Å]	1.442	1.440	1.443 (1.412)	1.439	1.440	1.439
C1–C7 [Å]	1.438	1.442	1.451 (1.423)	1.438	1.446	1.448
C1–C2 [Å]	1.440	1.433	1.426 (1.401)	1.439	1.440	1.431
C2–C3 [Å]				1.425	1.467	1.425
C3–C8 [Å]				1.443	1.447	1.445
C7–C8 [Å]	1.465	1.464	1.477 (1.452)	1.458	1.457	1.453
M–M [Å]	2.766	2.543	2.514 (2.538)	2.874	2.574	2.639
C3-C8-C7-C6 [°]	176	176	170 (170)	175	173	177

[a] $\delta = [(M-C7)-(M-C2)]/(M-C2)$.

depopulated. This is what happens in the singlet states of the *syn*-[(CpM)$_2$(C$_8$H$_6$)] (M = Mn, Cr, V) series, as illustrated by the MO diagrams shown in Figure 14. In the case of the 32-TNE model *syn*-[(CpMn)$_2$(η^5,η^5-C$_8$H$_6$)], the "t$_{2g}$" configuration can be written as $\sigma^2\pi_\perp{}^2\delta^2\sigma^{*2}\delta^{*2}\pi_\perp{}^0$. The existence of a weak π(Mn–Mn) single bond is consistent with a small HOMO–LUMO gap and with a singlet state computed to be only 0.07 eV more stable than the triplet state. Going from the singlet state of the manganese to the chromium derivative corresponds to the removal of two electrons from a b$_1$ MO which should be of σ*, δ*, or mixed σ*/δ* character (Scheme 7), but because of the significant tilting of the Cp ligands due to steric repulsion, it is now of a $\pi_\perp$* nature. This configuration is consistent with a weak π-type double bond. Owing to the very small HOMO–LUMO gap, the triplet state is found to be more stable than the singlet state by 0.16 eV. With two electrons less, the singlet state of *syn*-[(CpV)$_2$(η^5,η^5-C$_8$H$_6$)] has three vacant M–M antibonding orbitals of $\pi_\perp$*, $\pi_{//}$*, and δ* character (Figure 14). This result agrees with the description of a weak triple bond by Jones and O'Hare,[10b] although their description is of a σ/π/δ rather than of a $\pi_\perp/\pi_{//}/\delta$ bond. The optimized V–V distance in the singlet state (2.366 Å) is shorter than the experimental one (2.538 Å).[10b] Nevertheless, the triplet state is computed to be 0.31 eV more stable than the singlet state. This is in contrast to the fact that the compound is found to be antiferromagnetic with a singlet–triplet separation of ~0.17 eV.[10b]

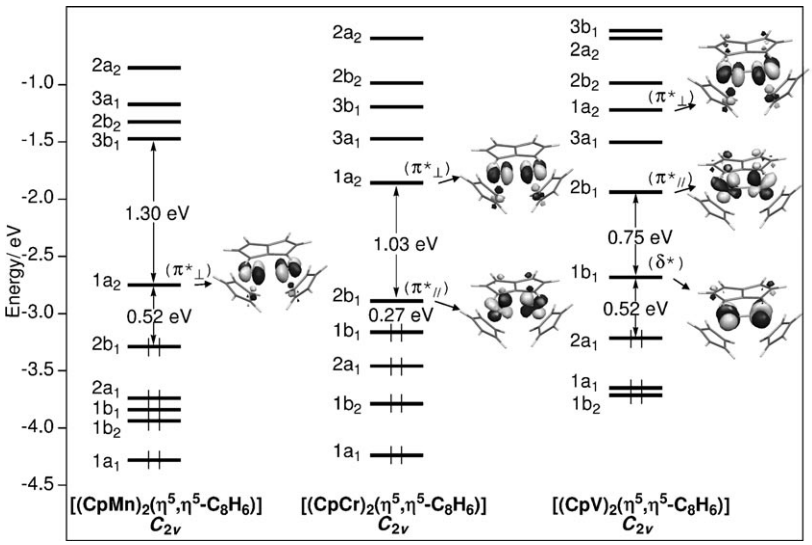

Figure 14. MO diagrams of *syn*-[(CpM)$_2$(C$_8$H$_6$)] (M = Mn, Cr, V) in the singlet state.

Surprisingly, the *syn*-[{(CO)$_3$M}$_2$(η^5,η^5-C$_8$H$_6$)] (M = Ti, V, Cr) series provided somewhat different results to those of the related isoelectronic CpM series. First, the geometry optimization of the singlet states within the C_{2v} symmetry constraint yielded a different "t$_{2g}$" electron configuration. In the case of the 32-TNE chromium derivative, the empty "t$_{2g}$" orbital is of b$_1$ symmetry and has a mixed σ*/δ* dominant character. It has little $\pi_{//}$* character since the (CO)$_3$Cr moieties do no bend like the CpM units. In the case of the 30-TNE vanadium model, the two empty orbitals are of a σ*/δ* and $\pi_\perp$* nature. In the case of the 28-TNE titanium species, the three empty orbitals are of σ*/δ, $\pi_\perp$*, and δ*/σ* character. Secondly, the C_{2v} geometry was found to be significantly unstable with respect to distortion towards C_2 symmetry (see Figure 13 and Table 8). This distortion corresponds to a rotation of the M(CO)$_3$ units around their C_3 rotational axes. Rotation releases the steric repulsion between the carbonyl groups and depends strongly on the M–M distance. Note that in the case of M = Mn or Re (34 TNEs; no metal–metal bond) the undistorted C_{2v} structure (Figure 10) is the energy minimum for the *syn* configuration (see above). Thus, in these 28-, 30-, and 32-TNE series, the steric repulsion between (CO)$_3$M units is released differently to that between CpM units. In the former case, the metal units rotate around their "vertical" axis, whereas in the latter case they bend away (Figure 13). With respect to metal–metal and metal–pentalene bonding, there is little difference between the C_{2v} and C_2 geometries of the (CO)$_3$M derivatives. With respect to the ground state, the vanadium derivative is computed to be diamagnetic while the titanium and chromium species exhibit a small singlet–triplet separation. In the former the triplet is computed to lie 0.11 eV above the singlet state, whereas in the latter it is found 0.09 eV below the singlet state.

[M$_2$(pentalene)$_2$] complexes: The first dinuclear bis-pentalene sandwich complexes to be observed, namely [Co$_2$(C$_8$H$_6$)$_2$] and [Ni$_2$(C$_8$H$_6$)$_2$], were reported in 1972 by Katz and co-workers.[4c,d] However, their structures were not fully elucidated. [Ni$_2$(C$_8$H$_6$)$_2$] was said to be of D_{2h} symmetry, at least over the average of the NMR timescale.[4c] The existence of [Rh$_2$(C$_8$H$_6$)$_2$] and [Pd$_2$(C$_8$H$_6$)$_2$] has also been briefly mentioned.[3d] The only example of this type of compound to be fully structurally characterized so far is [Mo$_2${η^5,η^5-C$_8$H$_4$(1,4-Si*i*Pr$_3$)$_2$}$_2$].[9c] This compound of near D_{2h} symmetry has a short Mo–Mo bond of 2.34 Å. Its electronic structure has been investigated by photoelectron spectroscopy and the data have been compared with DFT calculations on [Mo$_2$(C$_8$H$_6$)$_2$].[9g]

It is possible to build a simplified MO diagram for [M$_2$(η^5,η^5-C$_8$H$_6$)$_2$] of idealized D_{2h} symmetry based on symmetry and orbital frontier theory, in the same way as that in

Figure 11. This MO diagram is shown in Figure 15. The major bonding interactions are expected to occur between the 10 occupied pentalenic π-type combinations and 10

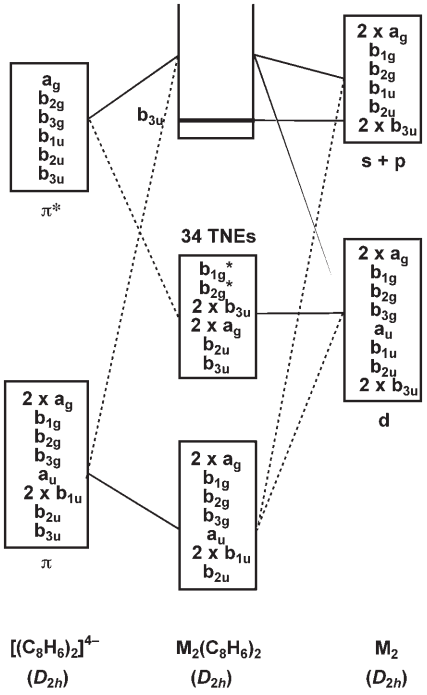

Figure 15. Simplified MO diagram for an $[M_2(\eta^5,\eta^5\text{-}C_8H_6)_2]$ species of idealized D_{2h} symmetry.

metal combinations of the same symmetry. It follows that eight of the 18 metal combinations should remain nonbonding. Since the metal s and p combinations are expected to interact preferentially with the ligands, seven of the eight metal–ligand nonbonding combinations should have a predominately d character, more or less stabilized by the π*(pentalene) levels. Only one of them (b_{3u}) should be of an s and p nature by symmetry. From the resulting MO diagram (Figure 15) one may expect this 34-TNE $[M_2(\eta^5,\eta^5\text{-}C_8H_6)_2]$ D_{2h} structure to have closed-shell stability, which would correspond to an 18-/16-MVE species, similar to the 34-MVE *anti*-$[(CpFe)_2(\eta^5,\eta^5\text{-}C_8H_6)]$ complex in Scheme 6. With more than 34 TNEs, partial pentalene decoordination is expected. With less than 34 TNEs, depopulation of the nonbonding d-block is likely to create metal–metal bonding and/or open shell situations. These d-type orbitals are sketched in Scheme 8. Three of them have a bonding phase relationship (σ, $\pi_\perp$, and δ) and another three are their antibonding counterparts (σ*, $\pi_\perp$*, and δ*). One antibonding combination ($\pi_{//}$*) has no d-block bonding counterpart. Indeed, the metal–metal bonding $\pi_{//}$ d-type combination (b_{1u}) is involved in metal–pentalene bonding (Figure 15). Depopulation of the σ*, $\pi_\perp$*, and $\pi_{//}$* MOs should induce significant metal–metal bonding, providing that the metal–pentalene interactions allow the metal atoms to approach each other. In order to test this qualitative model, geometry

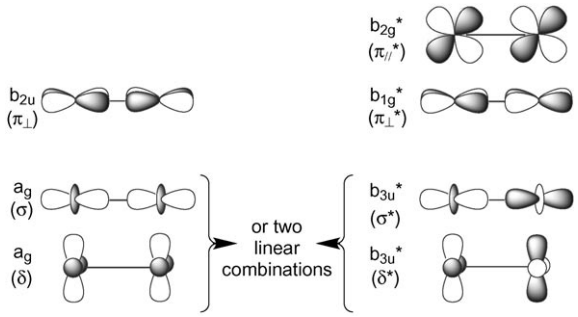

Scheme 8. The d-type orbitals present in pentalene dinuclear complexes with less than 34 TNEs.

optimizations have been performed on the $[M_2(C_8H_6)_2]$ (M = Cr, Mn, Fe, Co, Ni, Mo, Re, Ru, Rh, Pd) series. Some of the ground-state optimized structures are shown in Figure 16 and the major computed data are given in Table 9 and Table 10.

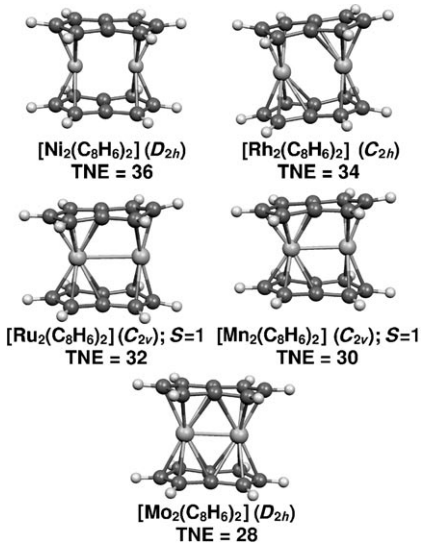

Figure 16. Optimized geometries of 28- to 36-TNE $[M_2(C_8H_6)_2]$ complexes in their lowest spin states.

34 TNEs: Geometry optimizations of $[M_2(C_8H_8)_2]$ (M = Co, Rh) complexes with D_{2h} symmetry constraints lead to the closed-shell electronic structure shown in Figure 15. The computed HOMO–LUMO gap is 0.79 and 1.40 eV for M = Co and Rh, respectively. With $\delta = 15$ and 16%, respectively, the coordination mode is of the η^5 type. Surprisingly, frequency calculations showed that the D_{2h} geometry is a transition state for both compounds. Further calculations showed the energy minimum to be of C_{2h} symmetry with each metal atom bonded in an η^5 fashion to one C_5 ring ($\delta = 4$–5%) and in an η^3 fashion ($\delta = 25$%) to the other ring (Figure 16, Table 9, and Table 10). The $[M_2(\eta^5,\eta^5\text{-}C_8H_8)_2]$ to $[M_2(\eta^5,\eta^3\text{-}C_8H_8)_2]$ distortion does not significantly modify the general MO diagram shown in Figure 15 (no level crossing). It provides a very small additional stabilization of 0.01

Table 9. Major computed data for the ground states of $[M_2(C_8H_6)_2]$ (M = Cr, Mn, Fe, Co, Ni).

	$[Cr_2(C_8H_6)_2]$ $S=1$ D_{2h}	$[Mn_2(C_8H_6)_2]$ $S=1$ C_{2v}		$[Fe_2(C_8H_6)_2]$ $S=1$ D_{2h}	$[Co_2(C_8H_6)_2]$ $S=0$ C_{2h}	$[Ni_2(C_8H_6)_2]$ $S=0$ D_{2h}
TNE	28	30		32	34	36
HOMO–LUMO gap [eV]					1.05	0.77
		Mn_1	Mn_2			
M−C7 [Å]	2.288	2.449	2.232	2.268	2.489	2.438
M−C1 [Å]	2.196	2.195	2.126	2.105	2.090	2.183
M−C2 [Å]	2.220	2.153	2.094	2.079	1.993	2.036
M−C7′ [Å]					2.149	
M−C1′ [Å]					2.099	
M−C2′ [Å]					2.076	
δ [%][a]	4	14	7	9	25 (η^3), 4 (η^5)	20
C−C(pentalene)						
average [Å]	1.446	1.447		1.449	1.447	1.442
C1−C7 [Å]	1.454	1.461		1.453	1.457	1.426
C1−C2 [Å]	1.434	1.437		1.442	1.444	1.446
C7−C8 [Å]	1.458	1.454		1.459	1.460	1.494
C4−C8 [Å]		1.441			1.436	
C4−C5 [Å]		1.444			1.443	
M–M [Å]	2.148	2.430		2.357	2.563	2.699
C3-C8-C7-C6 [°]	175	175		175	175	176
metal spin density	0.99	2.75	−0.55	1.12		

[a] $\delta = [(M-C7)-(M-C2)]/(M-C2)$.

Table 10. Major computed data for the ground states of $[M_2(C_8H_6)_2]$ (M = Mo, Re, Ru, Rh, Pd). Averaged available experimental values[9c] are given in parentheses.

	$[Mo_2(C_8H_6)_2]$ $S=0$ D_{2h}	$[Re_2(C_8H_6)_2]$ $S=1$ D_{2h}	$[Ru_2(C_8H_6)_2]$ $S=1$ C_{2v}		$[Rh_2(C_8H_6)_2]$ $S=0$ C_{2h}	$[Pd_2(C_8H_6)_2]$ $S=0$ D_{2h}
TNE	28	30	32		34	36
HOMO–LUMO gap [eV]	0.70				1.66	0.94
			Ru_1	Ru_2		
M−C7 [Å]	2.423 (2.360–2.432)	2.472	2.668	2.324	2.651	2.635
M−C1 [Å]	2.295 (2.263–2.298)	2.256	2.267	2.231	2.224	2.364
M−C2 [Å]	2.294 (2.258–2.260)	2.190	2.150	2.169	2.118	2.193
M−C7′ [Å]					2.323	
M−C1′ [Å]					2.237	
M−C2′ [Å]					2.210	
δ [%][a]	6	13	24	7	25 (η^3), 5 (η^5)	20
C−C(pentalene)						
average [Å]	1.453 (1.430–1.464)	1.456	1.448		1.449	1.435
C1−C7 [Å]	1.461 (1.445–1.476)	1.456	1.464		1.462	1.421
C1−C2 [Å]	1.443 (1.410–1.453)	1.456	1.443		1.448	1.446
C7−C8 [Å]	1.461 (1.447–1.458)	1.453	1.453		1.452	1.493
C4−C8 [Å]			1.433		1.440	
C4−C5 [Å]			1.448		1.445	
M–M [Å]	2.370 (3.340)	2.478	2.741		2.736	2.843
C3-C8-C7-C6 [°]	177 (179–176)	172	176		176	176
metal spin density		0.77	1.54	0.43		

[a] $\delta = [(M-C7)-(M-C2)]/(M-C2)$.

and 0.04 eV for M = Co and M = Rh, respectively. This hardly significant value is indicative of a particularly flat potential energy surface that is associated with the displacement of metal atoms around their equilibrium positions. The $[M_2(\eta^5,\eta^3\text{-}C_8H_8)_2]$ architecture can be described as an 18-/16-MVE species made of two ML_5 units with no significant metal–metal interaction. This is a favorable closed-shell electron count, in agreement with the fact that these compounds have already been observed.[4d,3d] They should be stable enough to be fully structurally characterized.

36 TNEs: Geometry optimization of $[Ni_2(C_8H_8)_2]$ showed the ideal D_{2h} structure to be a minimum with an η^3 bonding mode for each C_5 ring (Figure 16 and Table 9). It is thus tempting to describe this $[M_2(\eta^3,\eta^3\text{-}C_8H_8)_2]$ ($M^{II}=d^8$) structure as consisting of two independent 16-MVE units of the well-known $[M(\eta^3\text{-allyl})_2]$ type. It turns out that this is not completely the case because the C7−C8 "double bonds" are not innocent in this matter. Indeed, group theory predicts that going from the 34-TNE species depicted in Figure 15 to a 36-TNE species consisting of two noninteracting $[M(\eta^3$-

allyl)$_2$] 16-MVE units would require the b_{1u} supplementary level to be filled, however, calculations indicate that the level which is actually filled has b_{3g} symmetry. This "level crossing" results from π conjugation within the $C_8H_6^{2-}$ ligand which cannot simply be described as being made of two allyl anions bridged by a double bond. The moderate computed HOMO–LUMO gap (Table 9) suggests moderate stability for these species which have been observed, but not structurally characterized.[4c,3d]

Exploratory calculations indicate that, as for the related 34-MVE species, the potential energy surface of the 36-MVE [$Ni_2(C_8H_8)_2$] complex is rather flat around its minimum. This feature is even more pronounced for the isoelectronic [$Pd_2(C_8H_8)_2$] complex for which the [Pd(η^3-allyl)$_2$] D_{2h} structure, isoelectronic with [Ni(η^3-allyl)$_2$], was found not to be a minimum. The computed minimum, characterized by frequency calculations, has a structure of C_s symmetry which can be averaged to D_{2h} and which is found to be only 0.03 eV more stable than the latter, a hardly significant value. This result is indicative of a large geometrical flexibility for this species. Only the results corresponding to the D_{2h} structure are reported in Table 10.

28, 30, and 32 TNEs: We start with a known 28-TNE molybdenum derivative[9c] whose electronic structure has been investigated by performing DFT calculations on the [$Mo_2(C_8H_6)_2$] model.[9g] Unsurprisingly, our calculations on [$Mo_2(C_8H_6)_2$] revealed a similar optimized [$Mo_2(\eta^5,\eta^5\text{-}C_8H_6)_2$] structure of D_{2h} symmetry and an ordering of levels similar to that found by Cloke et al.[9g] The MO diagram of [$Mo_2(C_8H_6)_2$] is derived from the general diagram of the 34-MVE species sketched in Figure 15 by depopulating the three top MOs of the d-block, namely b_{1g}* ($\pi_\perp$*), b_{2g}* ($\pi_{//}$*), and b_{3u}* (σ*). The corresponding d-type electron configuration is $(\sigma)^2(\pi_\perp)^2(\delta)^2(\delta^*)^2(\sigma^*)^0(\pi_{//}^*)^0(\pi_\perp^*)^0$. Since the bonding counterpart of $\pi_{//}$* is not a member of the d-block but is involved in metal–pentalene bonding (see above), we propose a Mo–Mo bond order of $2+\alpha$ ($\alpha<1$). Incidentally, a bond order of three would achieve the 18-/16-MVE count which is the most favored for dinuclear complexes of pentalene. The proposed bond order is consistent with the optimized Mo–Mo distance (2.37 Å), which is close to the experimental value found for [$Mo_2\{\eta^5,\eta^5\text{-}C_8H_4(1,4\text{-}Si\mathit{i}Pr_3)_2\}_2$] (2.34 Å).[9c] The diamagnetic behavior reported for this latter compound agrees with the moderate but significant HOMO–LUMO gap computed for [$Mo_2(C_8H_6)_2$] (0.70 eV). Consistent with this, the triplet state was found to be 0.45 eV less stable than the singlet state. Changing molybdenum to chromium switches the order of energy of the singlet and triplet states. In [$Cr_2(C_8H_6)_2$], the singlet state lies 0.18 eV above the triplet state which corresponds to $(\sigma)^2(\pi_\perp)^2(\delta)^2(\delta^*)^1(\sigma^*)^1(\pi_{//}^*)^0(\pi_\perp^*)^0$. This is due to a weaker metal–metal overlap which renders the σ* LUMO of the singlet state even less antibonding than in the molybdenum compound. Considering that the δ* MO is nonbonding for the actual Cr–Cr bond distances (2.14 and 2.16 Å in the singlet and triplet states, respectively), the formal Cr–Cr bond order is $2+\alpha$ and $1.5+\alpha$ in the singlet and triplet states, respectively. Note that an isoelectronic complex was characterized a long time ago by Jonas et al., namely [V_2(indenyl)$_2$].[23] Its X-ray structure exhibits a V–V distance of 2.351 Å and the compound is diamagnetic. It is likely to have the same ground-state configuration as [$Mo_2(C_8H_6)_2$].

With two more electrons, [$Re_2(C_8H_6)_2$] is found to adopt a D_{2h} structure (Table 10) and has a triplet ground state computed to be more stable than the singlet state by 0.25 eV. The triplet configuration is $(\sigma)^2(\pi_\perp)^2(\delta)^2(\delta^*)^2(\sigma^*)^1(\pi_{//}^*)^1(\pi_\perp^*)^0$, which corresponds to a formal Re–Re bond order of $1+\alpha$, in agreement with a rather short internuclear distance (2.478 Å). This metal–metal interaction is much weaker in [$Mn_2(C_8H_6)_2$] which also has a triplet ground state but which adopts a C_{2v} structure (Figure 16) in which one metal (Mn_2 in Table 9) atom is bonded in an η^5 symmetrical fashion to both ligands while the other one (Mn_1) is bonded in a more unsymmetrical η^5 fashion, tending slightly towards η^3. The computed triplet–singlet energy difference is 0.24 eV. The C_{2v}/D_{2h} energy difference in the triplet ground state is 0.10 eV. Interestingly, the 32-TNE [$Ru_2(C_8H_6)_2$] species adopts the same C_{2v} geometry as [$Mn_2(C_8H_6)_2$], but with a clearer tendency for Ru_1 to be η^3-bonded to both ligands (Figure 16 and Table 10). It also has a triplet ground state that is more stable than the singlet state by 0.20 eV and more stable than the D_{2h} triplet ground state by 0.29 eV. On the other hand, the isoelectronic [$Fe_2(C_8H_6)_2$] model adopts a D_{2h} symmetry with a triplet ground state corresponding to the $(\sigma)^2(\pi_\perp)^2(\delta)^2(\delta^*)^2(\pi_{//}^*)^2(\sigma^*)^1(\pi_\perp^*)^1$ configuration, that is, an Fe–Fe bond order of $0.5+\alpha/2$, in agreement with an internuclear separation of 2.357 Å. The singlet state is computed to be less stable by 0.51 eV.

Conclusion

Herein we have investigated the coordination ability of pentalene to bind to one and two transition metal atoms in compounds of the type [CpM(C_8H_6)], [(CO)$_3$M(C_8H_6)], [M(C_8H_6)$_2$], [(CpM)$_2$(C_8H_6)], [{(CO)$_3$M}$_2$(C_8H_6)], and [$M_2(C_8H_6)_2$] with different electron counts. The bonding in all the currently known compounds has been rationalized, as well as in (so far) hypothetical stable complexes. For example, diamagnetic compounds of the type (or isoelectronic with) [(CO)$_3$Fe(pentalene)], [(CO)$_3$Ni(pentalene)], [Cr(pentalene)$_2$], [{(CO)$_3$Ni}$_2$(pentalene)], [{(CO)$_3$V}$_2$(pentalene)], [Rh_2(pentalene)$_2$], and [Pd_2(pentalene)$_2$] should be stable enough to be isolated. Depending on the electron count and the nature of the metal(s), η^2 (predicted), η^3, η^5, η^8, or intermediate coordination modes can be adopted. In the case of mononuclear species, the most favored closed-shell electron counts are 18 and 16 MVEs. In the case of dinuclear species, an electron count of 34 MVEs is most favored. However, other electron counts can be stabilized, especially in the case of dinuclear complexes. Coordinated pentalene should most often be considered as formally being a dianion, but sometimes as a neutral ligand. In the former case it can

behave as an aromatic species made of two equivalent fused rings (Scheme 1), as a fivefold aromatic ring connected to an allylic anion (see one of the canonical formulae of Scheme 1), or even as two allylic anions bridged by a C7=C8 double bond. In the latter case, it can behave as a bond-alternating cyclic polyene (Scheme 1) or as a five-fold aromatic ring connected to an allylic cation. We are currently exploring the dynamics of some of the compounds studied, as well as extending this study to real and hypothetical complexes of related ligands such as anthracene, fluorenyl, or acepentalene.

Computational Details

Density functional theory (DFT) calculations were carried out using the Amsterdam density functional (ADF) program,[24] developed by Baerends and co-workers.[25] Electron correlation was treated within the local density approximation (LDA) within the Vosko–Wilk–Nusair parametrization.[26] The nonlocal corrections of Becke and Perdew were incorporated into the exchange and correlation energies, respectively.[27,28]

The numerical integration procedure applied in the calculations was developed by te Velde et al.[25e] The electronic configurations of atoms were described by a triple-ζ Slater-type orbital (STO) basis set for H 1s, C 2s and 2p, N 2s and 2p, O 2s and 2p, and P 3s and 3p augmented with a 3d single-ζ polarization for the C, N, O, and P atoms and with a 2p single-ζ polarization for the H atoms. A triple-ζ STO basis set was used for Ti, V, Cr, Mn, Fe, Co, and Ni 3d and 4s, and for Zr, Mo, Ru, Rh, and Pd 4d and 5s augmented with a single-ζ 4p polarization function for metals of the first row of the periodic table and a single-ζ 5p polarization function for the second row. A double-ζ STO basis set was used for Re and Os 5s and a triple-ζ STO basis set was used for Re and Os 4f, 5p, and 5d augmented with a single-ζ 6p polarization function. A frozen-core approximation was used to treat the core shells up to 1s for C, N and O, 2p for P, 3p for the metal atoms of the first row, 4p for the second row, and 4d for Re and Os.[25] For systems containing atoms for which Z is greater than 41, the scalar relativistic (SR) ZORA (zero-order regular approximation) was used (with the associated optimized valence basis set).[29] Full geometry optimizations were carried out using the analytical gradient method implemented by Verluis and Ziegler.[30] Spin-unrestricted calculations were performed for all the open-shell systems. Frequency calculations[31] were performed on all the studied compounds, except for $[CpFe(\eta^5\text{-}C_8H_4Fc_2)]^+$. Unless specified in the text or just below, the molecular structures described correspond to characterized energy minima. In a few cases, for the sake of simplicity, the structures described have a higher symmetry and almost the same energy (within 0.03 eV) as the C_1 geometry which was found to be the minimum. In such cases, both structures differ by a simple rotation of the $M(CO)_3$ or MCp moiety. It has been checked that the averaged C_1 geometry is not significantly different to that described in the paper. These particular compounds are $[(CO)_3Cr(C_8H_6)]$, *syn*-$[(CpV)_2(C_8H_6)]$, and *anti*-$[(CpM)_2(C_8H_8)]$ (M = Fe, Co, Ni). The molecular structures and orbitals were represented using MOLEKEL4.1.[32]

Acknowledgements

Computing facilities were provided by the University of Rennes 1 (PCIO) and the CNRS (IDRIS national computing center).

[1] For selected papers on the electronic structure of pentalene and its derivatives, see: a) Y. Jean, *New J. Chem.* **1980**, *4*, 11–15; b) A. Toyota, S. Koseki, *J. Phys. Chem.* **1996**, *100*, 2100–2106; c) T. Bally, S. Chai, M. Neuenschwander, Z. Zhu, *J. Am. Chem. Soc.* **1997**, *119*, 1869–1875; d) A. Falchi, C. Gellini, P. R. Salvi, K. Hafner, *J. Phys. Chem.* **1995**, *99*, 14659–14666; e) A. Falchi, C. Gellini, P. R. Salvi, K. Hafner, *J. Phys. Chem.* **1998**, *102*, 5006–5012; f) A. Falchi, C. Gellini, P. R. Salvi, K. Hafner, *J. Phys. Chem.* **2000**, *104*, 1078; g) M. J. Bearpark, F. Bernardi, M. Olivucci, M. A. Robb, *Int. J. Quant. Chem.* **1996**, *60*, 505–512; h) M. J. Bearpark, M. A. Robb, *J. Chem. Phys.* **2000**, *104*, 1075–1077; i) M. J. Bearpark, L. Blancafort, M. A. Robb, *Mol. Phys.* **2002**, *100*, 1735–1739.

[2] a) T. J. Katz, M. Rosenberger, *J. Am. Chem. Soc.* **1962**, *84*, 865–866; b) T. J. Katz, M. Rosenberger, R. K. O'Hara, *J. Am. Chem. Soc.* **1964**, *86*, 249–252; c) J. J. Stezowski, D. Wilhelm, T. Clark, P. von - Ragué Schleyer, *J. Chem. Soc. Chem. Commun.* **1985**, 1263–1264; d) T. K. Zywietz, H. Jiao, P. von Ragué Schleyer, *J. Org. Chem.* **1998**, *63*, 3417–3422; e) M. Nakano, S. Kiribayashi, S. Yamada, I. Shigemoto, K. Yamagushi, *Chem. Phys. Lett.* **1996**, *262*, 66–73; f) F. N. Cloke, C. Kuchta, R. M. Harker, P. B. Hitchcock, J. S. Parry, *Organometallics* **2000**, *19*, 5795–5798.

[3] a) S. A. R. Knox, F. G. A. Stone, *Acc. Chem. Res.* **1974**, *7*, 312–328; b) M. Akita, Organometallic News, **1995**, *2*, 47; c) H. Butenschön, *Angew. Chem.* **1997**, *109*, 1771–1773; *Angew. Chem. Int. Ed. Engl.* **1997**, *36*, 1695–1697; d) F. G. N. Cloke, *Pure Appl. Chem.* **2001**, *73*, 233–238.

[4] a) T. J. Katz, M. Rosenberg, *J. Am. Chem. Soc.* **1963**, *85*, 2030–2031; b) T. J. Katz, J. J. Mrowa, *J. Am. Chem. Soc.* **1967**, *89*, 1105–1111; c) T. J. Katz, N. Acton, *J. Am. Chem. Soc.* **1972**, *94*, 3281–3283; d) T. J. Katz, N. Acton, J. McGinnis, *J. Am. Chem. Soc.* **1972**, *94*, 6205–6206.

[5] W. Weidemueller, K. Hafner, *Angew. Chem.* **1973**, *85*, 958–959; *Angew. Chem. Int. Ed. Engl.* **1973**, *12*, 925.

[6] a) A. Brookes, J. Howard, S. A. R. Knox, F. G. A. Stone, P. Woodward, *J. Chem. Soc. Chem. Commun.* **1973**, 587–589; b) S. A. R. Knox, R. P. Phillips, F. G. A. Stone, *J. Chem. Soc. Dalton Trans.* **1974**, 658–661; c) J. A. K. Howard, S. A. R. Knox, V. Riera, F. G. A. Stone, P. Woodward, *J. Chem. Soc. Chem. Commun.* **1974**, 452–453; d) J. A. K. Howard, S. A. R. Knox, V. Riera, F. G. A. Stone, A. C. Szary, *J. Chem. Soc. Chem. Commun.* **1974**, 788–789; e) J. A. K. Howard, S. A. R. Knox, R. J. McKinney, R. F. D. Stansfield, F. G. A. Stone, P. Woodward, *J. Chem. Soc. Chem. Commun.* **1976**, 557–558; f) P. J. Harris, J. A. K. Howard, S. A. R. Knox, R. J. McKinney, R. P. Phillips, F. G. A. Stone, P. Woodward, *J. Chem. Soc. Dalton Trans.* **1978**, 403–412; g) J. A. K. Howard, P. Woodward, *J. Chem. Soc. Dalton Trans.* **1978**, 412; h) S. A. R. Knox, R. J. McKinney, V. Riera, F. G. A. Stone, A. Szary, *J. Chem. Soc. Dalton Trans.* **1979**, 1801–1811; i) S. A. R. Knox, R. J. McKinney; F. G. A. Stone, *J. Chem. Soc. Dalton Trans.* **1980**, 235–239.

[7] a) E. E. Bunel, L. Valle, N. L. Jones, P. J. Carrol, C. Barra, M. González, N. Muñoz, G. Visconti, A. Aizman, J. M. Manríquez, *J. Am. Chem. Soc.* **1988**, *110*, 6596–6598; b) W. M. Reiff, J. M. Manríquez, J. S. Miller, *Hyperfine Interact.* **1990**, *53*, 397–402; c) B. Oelcklers, I. Chávez, J. M. Manríquez, E. Román, *Organometallics* **1993**, *12*,

3396–3397; d) J. M. Manríquez, M. D. Ward, W. M. Reiff, J. C. Calabrese, N. L. Jones, P. J. Carroll, E. E. Bunel, J. S. Miller, *J. Am. Chem. Soc.* **1995**, *117*, 6182–6193; e) A. Alvarez-Larena, J. L. Briansó, J. F. Piniella, J. Farran, J. M. Manríquez, I. Chávez, B. Oëlckers, E. Molins, C. Miravitlles, *Acta Crystallogr. Sect. C* **1996**, *52*, 2754–2757; f) C. Miravitlles, E. Molins, W. Maniukiewicz, M. Mas, J. M. Manríquez, I. Chávez, B. Oëlckers, A. Alvarez-Larena, J. L. Briansó, *Acta Crystallogr. Sect. C* **1996**, *52*, 3047–3049; g) Y. Portilla, I. Chávez, V. Arancibia, B. Loeb, J. M. Manríquez, *Inorg. Chem.* **2002**, *41*, 1831–1836; h) F. Burgos, I. Chávez, J. M. Manriquez, M. Valderrama, E. Lago, E. Molins, F. Delpech, A. Castel, P. Rivière, *Organometallics* **2001**, *20*, 1287–1291.

[8] a) K. Jonas, B. Gabor, R. Mynott, K. Angermund, O. Heinemann, C. Krüger, *Angew. Chem.* **1997**, *109*, 1790–1793; *Angew. Chem. Int. Ed. Engl.* **1997**, *36*, 1712–1714; b) K. Jonas, P. Kolb, G. Kollbach, B. Gabor, R. Mynott, K. Angermund, O. Heinemann, C. Kruger, *Angew. Chem.* **1997**, *109*, 1793–1796; *Angew. Chem. Int. Ed. Engl.* **1997**, *36*, 1714–1718; c) B. Gabor, K. Jonas, R. Mynott, *Inorg. Chim. Acta* **1998**, *270*, 555–558; d) R. Gleiter, S. Bethke, J. Okubo, K. Jonas, *Organometallics* **2001**, *20*, 4274–4278.

[9] a) Q. A. Abbasali, F. G. N. Cloke, P. B. Hitchcock, S. C. P. Joseph, *Chem. Commun.* **1997**, 1541–1542; b) F. G. N. Cloke, P. B. Hitchcock, *J. Am. Chem. Soc.* **1997**, *119*, 7899–7900; c) M. C. Kuchta, F. G. N. Cloke, P. B. Hitchcock, *Organometallics* **1998**, *17*, 1934–1936; d) F. G. N. Cloke, J. C. Green, C. N. Jardine, *Organometallics* **1999**, *18*, 1080–1086; e) F. G. N. Cloke, J. C. Green, C. N. Jardine, M. C. Kuchta, *Organometallics* **1999**, *18*, 1087–1090; f) F. G. N. Cloke, P. B. Hitchcock, *J. Am. Chem. Soc.* **2002**, *124*, 9352–9353; g) F. G. N. Cloke, J. C. Green, N. Kaltsoyannis, *Organometallics* **2004**, *23*, 832–835.

[10] a) S. C. Jones, T. Hascall, S. Barlow, D. O'Hare, *J. Am. Chem. Soc.* **2002**, *124*, 11610–11611; b) S. C. Jones, D. O'Hare, *Chem. Commun.* **2003**, 2208–2209; c) S. C. Jones, T. Hascall, A. J. Norquist, D. O'Hare, *Inorg. Chem.* **2003**, *42*, 7707–7709.

[11] a) M. T. Garland, J.-Y. Saillard, I. Chávez, B. Oëlckers, J.-M. Manríquez, *J. Mol. Struct.* **1997**, *390*, 199–208; b) K. Costuas, J.-Y. Saillard, *Chem. Commun.* **1998**, 2047–2048.

[12] T. A. Albright, P. Hofmann, R. Hoffmann, C. P. Lillya, P. A. Dobosh, *J. Am. Chem. Soc.* **1983**, *105*, 3396–3411.

[13] J. K. Burdett, E. Canadell, *Organometallics* **1985**, *4*, 805–815.

[14] M.-D. Su, S.-Y. Chu, *Chem. Phys. Lett.* **1998**, *298*, 107–112.

[15] R. B. King, *Appl. Organomet. Chem.* **2003**, *17*, 393–397.

[16] a) T. Ziegler, A. Rauk, *Theor. Chim. Acta* **1977**, *46*, 1–10; b) T. Ziegler, "Qualitative Results and Qualitative Analysis by the Hartree–Fock–Slater Transition State Method" in *Quantum Chemistry: The Challenge of Transition Metals and Coordination Chemistry* (Ed.: A. Veillard), NATO ASI, D. Reidel, Dordrecht, The Netherlands, **1986**.

[17] a) T. J. Katz, M. Rosenberg, *J. Am. Chem. Soc.* **1963**, *85*, 2030–3031; b) E. Molins, W. Maniukiewicz, C. Miravitlles, M. Mas, J. M. Manríquez, I. Chávez, B. Oëlcklers J. Farrin, J. L. Briansó, *Acta Crystallogr., Sect. C* **1996**, *52*, 2414–2416.

[18] J. Lukasser, H. Angleitner, H. Schottenberger, H. Kopacka, M. Schweiger, B. Bildstein, K.-H. Ongania, K. Wurst, *Organometallics* **1995**, *14*, 5566–5578.

[19] a) M. J. Calhorda, L. F. Veiros, *J. Organomet. Chem.* **2001**, *635*, 197–203; b) M. J. Calhorda, L. F. Veiros, *Inorg. Chim. Acta* **2003**, *350*, 547–556; c) M. J. Calhorda, V. Félix, L. F. Veiros, *Coord. Chem. Rev.* **2002**, *230*, 49–64; d) M. J. Calhorda, C. C. Romão, L. F. Veiros, *Chem. Eur. J.* **2002**, *8*, 868–875.

[20] a) C. A. Bradley, I. Keresztes, E. Lobkovsky, V. G. Young, P. J. Chirik, *J. Am. Chem. Soc.* **2004**, *126*, 16937–16950; b) L. F. Veiros, *Chem. Eur. J.* **2005**, *11*, 2505–2518.

[21] M. R. Churchill, G. L. Kuo-Kuang, *Inorg. Chem.* **1973**, *12*, 2274.

[22] T. A. Albright, J. K. Burdett, M.-H. Whangbo, *Orbital Interactions in Chemistry*, Wiley, New York, **1985**.

[23] K. Jonas, W. Rüsseler, C. Krüger, E. Raabe, *Angew. Chem.* **1986**, *98*, 905; *Angew. Chem. Int. Ed. Engl.* **1986**, *25*, 928–929.

[24] ADF2002.01, Vrije Universiteit, Amsterdam, The Netherlands, SCM.

[25] a) E. J. Baerends, D. E. Ellis, P. Ros, *Chem. Phys.* **1973**, *2*, 41; b) G. te Velde, E. J. Baerends, *J. Comput. Phys.* **1992**, *99*, 84; c) C. Fonseca Guerra, J. G. Snijders, G. te Velde, E. J. Baerends, *Theor. Chim. Acc.* **1998**, *99*, 391; d) F. M. Bickelhaupt, E. J. Baerends, *Rev. Comput. Chem.* **2000**, *15*, 1; e) G. te Velde, F. M. Bickelhaupt, C. Fonseca Guerra, S. J. A. van Gisbergen, E. J. Baerends, J. G. Snijders, T. Ziegler, *J. Comput. Chem.* **2001**, *22*, 931.

[26] S. D. Vosko, L. Wilk, M. Nusair, *Can. J. Chem.* **1990**, *58*, 1200.

[27] a) A. D. Becke, *J. Chem. Phys.* **1986**, *84*, 4524; b) A. D. Becke, *Phys. Rev. A* **1988**, *38*, 3098.

[28] a) J. P. Perdew, *Phys. Rev. B* **1986**, *33*, 8822; b) J. P. Perdew, *Phys. Rev. B* **1986**, *34*, 7406.

[29] E. van Lenthe, A. W. Ehlers, E. J. Baerends, *J. Chem. Phys.* **1999**, *110*, 8943.

[30] L. Verluis, T. Ziegler, *J. Chem. Phys.* **1988**, *88*, 322.

[31] a) L. Fan, T. Ziegler, *J. Chem. Phys.* **1992**, *96*, 9005; b) L. Fan, T. Ziegler, *J. Phys. Chem.* **1992**, *96*, 6937.

[32] P. Flükiger, H. P. Lüthi, S. Portmann, J. Weber, MOLEKEL4.1, Swiss Center for Scientific Computing (CSCS), Switzerland, **2000–2001**.

Received: July 3, 2005
Published online: December 15, 2005

